POLITECNICO DI TORINO
Repository ISTITUZIONALE

Nonlinear thermal stresses analysis and post-buckling of rectangular composite laminates using high-order plate finite elements

Original
Nonlinear thermal stresses analysis and post-buckling of rectangular composite laminates using high-order plate finite elements / Pagani, A., Bracaglia, F., Zappino, E., Carrera, E.. - In: JOURNAL OF THERMAL STRESSES. - ISSN 0149-5739. - 49:10(2026), pp. 1555-1581. [10.1080/01495739.2026.2676322]

Availability:
This version is available at: 11583/3013177 since: 2026-07-16T09:55:00Z

Publisher:
Taylor and Francis

Published
DOI:10.1080/01495739.2026.2676322

Terms of use:

This article is made available under terms and conditions as specified in the corresponding bibliographic description in the repository

Publisher copyright

(Article begins on next page)

07 November 2026



Journal of Thermal Stresses

ISSN: 0149-5739 (Print) 1521-074X (Online) Journal homepage: www.tandfonline.com/journals/uths20

Nonlinear thermal stresses analysis and post-buckling of rectangular composite laminates using high-order plate finite elements

Alfonso Pagani, Francesca Bracaglia, Enrico Zappino & Erasmo Carrera

To cite this article: Alfonso Pagani, Francesca Bracaglia, Enrico Zappino & Erasmo Carrera (2026) Nonlinear thermal stresses analysis and post-buckling of rectangular composite laminates using high-order plate finite elements, Journal of Thermal Stresses, 49:10, 1555-1581, DOI: 10.1080/01495739.2026.2676322

To link to this article: https://doi.org/10.1080/01495739.2026.2676322

© 2026 The Author(s). Published with license by Taylor & Francis Group, LLC

Published online: 01 Jun 2026.

Submit your article to this journal

Article views: 299

View related articles

View Crossmark data

Citing articles: 3 View citing articles

Full Terms & Conditions of access and use can be found at https://www.tandfonline.com/action/journalInformation?journalCode=uths20

JOURNAL OF THERMAL STRESSES
2026, VOL. 49, NO. 10, 1555–1581
https://doi.org/10.1080/01495739.2026.2676322

Taylor & Francis
by informa

OPEN ACCESS Check for updates

Nonlinear thermal stresses analysis and post-buckling of rectangular composite laminates using high-order plate finite elements

Alfonso Pagani, Francesca Bracaglia, Enrico Zappino, and Erasmo Carrera

Mul2 Lab, Department of Mechanical and Aerospace Engineering, Politecnico di Torino, Torino, Italy

ABSTRACT

The present paper investigates the geometrically nonlinear thermo-elastic response of composite plates undergoing large rotations/displacements, with a focus on post-buckling and 3D thermal stresses. The governing equations are derived from the Principle of Virtual Displacement (PVD), whereby the full Green-Lagrange strain tensor is adopted in a total Lagrangian framework. The thermal load is described using a decoupled approach, and constant thermal distribution is considered. The employed plate elements are developed through the Carrera Unified Formulation (CUF) and their formal expression is independent of the theory approximation order. Thus, low-order equivalent-single-layer (ESL) to high-order layer-wise (LW) models can be implemented with ease. The nonlinear problem is solved through the Newton-Raphson procedure combined with the arc-length constraint. Plates with different geometries and materials are analyzed, and linear and nonlinear analyses are compared. From the results, it is shown that LW models are needed to describe the 3D thermal stresses in nonlinear equilibrium states, whereas ESL finite elements are enough to describe the global deformation state.

ARTICLE HISTORY
Received 27 March 2025
Accepted 12 May 2026

KEYWORDS
Green-Lagrange strain tensor; nonlinear analysis; nonlinear stresses; thermal post-buckling; thermal stresses; thermo-elastic nonlinear analysis

1. Introduction

Aerospace structures operate in harsh environments. For example, severe thermal loads can challenge the design of reentry vehicles, supersonic aircraft, large antennas, space reflectors, etc. To reduce weight and volume, thin-walled structures are used in the design of the above components [1,2], and for such structures, temperature variation is a significant loading factor whose influence cannot be ignored [3,4]. Under certain circumstances and boundary conditions, thermal loading can lead to buckling and post-buckling of thin-walled components.

To describe and design the thin-walled components, the use of classical linear analysis methods is no longer sufficient. As a consequence, the definition of accurate and reliable models which are not restricted to the assumption of small displacements and rotations, becomes necessary [5]. Large deformations couple bending, torsion, shear, and extension and cause deformation-induced membrane forces [6]; additionally, the increase in temperature of the structural components can result in buckling and high-nonlinear phenomena [7,8]. While, the pure mechanical behavior of the structures in large-displacement and nonlinear conditions has been extensively studied [9–12], less attention has been paid to the description of thermal loading.

CONTACT Alfonso Pagani alfonso.pagani@polito.it Mul2 Lab, Department of Mechanical and Aerospace Engineering, Politecnico di Torino, Corso Duca degli Abruzzi 24, Torino 10129, Italy.

© 2026 The Author(s). Published with license by Taylor & Francis Group, LLC
This is an Open Access article distributed under the terms of the Creative Commons Attribution License (http://creativecommons.org/licenses/by/4.0/), which permits unrestricted use, distribution, and reproduction in any medium, provided the original work is properly cited. The terms on which this article has been published allow the posting of the Accepted Manuscript in a repository by the author(s) or with their consent.

The linear static thermo-elastic problem was vastly investigated using classical and high-order theories [13–16]. In the literature, the thermo-elastic instability has been widely investigated through a linearized formulation, and the problem was solved by knowing the critical temperature. Some examples are reported here, where different theories and models are adopted [17–20]. All these works introduced the geometrically nonlinear component in the description of the structure, followed by a linearization to obtain the bifurcation point. However, this method is only valid in case of stable pre-buckling and cannot be used to describe post-buckling behavior, large displacement, and related stresses in the plate. Indeed, for symmetric or angle-ply antisymmetric plates it is demonstrated that the linearized solution is an excellent method to define the critical temperature. However, when bending appears in linear range (e.g., in the case of non-uniform temperature distribution or asymmetric laminations), the linearization of the problem is not reliable, and the bifurcation-type instability is questionable [21,22].

A fully nonlinear formulation is mandatory in the description of post-buckling conditions or when high deflection and rotations are involved. Different theories and models that incorporate the geometrical nonlinearities inside the problem have been developed, and few works describing the nonlinear behavior of plates under thermal load have been published. Among these works, a direct iterative procedure was employed by Singh et al. [23] and Maloy et al. [24] whereas an eigenvalue-type procedure is employed in the nonlinear context. The post-buckling problem was solved by Sreehari et al. [25], with an analogous direct iterative process where the structural model was obtained through Inverse Hyperbolic Shear Deformation Theory (IHSDT) and the hygrothermal environment was also considered. Chen and Chen [26] employed a similar iterative procedure; they investigated the behavior of composite laminated plates under uniform thermal loading, considering the temperature-dependent properties of materials. Huang et al. [27] studied the post-buckling behavior of laminated plates under uniform temperature distribution through an incremental thermal loading procedure. With this approach, they minimized the total potential energy and described the equilibrium path in terms of displacements of the plate. Meyers and Hyer [28] analyzed different laminated plates, describing their buckling and post-buckling behavior using variational methods in conjunction with a Rayleigh-Ritz formulation, solving the nonlinear equations with a sequence of incremental temperature changes.

Over the years, many works have been published using different plate theories, and solution methods. However, in must of these works, the nonlinear terms are derived by describing the nonlinearities through the von Kármán strain displacement relations in conjunction with classical theories or simplified high-order theories. Von Kármán strains are often used to account for these geometrical nonlinearities and are developed specifically for the analysis of plates but the simplifications are justified only for moderate displacement and rotations. The use of the full Green-Lagrange strain tensor is recommended for a more accurate description of the nonlinearities as highlighted in [29] where the geometrically nonlinear problem is formulated for the mechanical load within the Carrera Unified Formulation (CUF) framework.

The Green-Lagrange strain tensor was applied to the nonlinear thermo-elastic problem by Panda and Singh [30], who obtained the governing equations of panels by minimizing the energy expression. High-order theories for the displacement component u_x and u_y were employed, and the solution was found through an iterative procedure that used the linearized buckling solution to build the nonlinear matrices, as a consequence, the stretching terms were neglected.

All the works above describe the thermo-elastic problem of the plate with some simplification on the nonlinearity description, either in terms of kinematic theory or in the solution procedure. They always describe the equilibrium curve of the plate under the thermal load but the post-buckling description of stresses is not reported. To the best of the authors' knowledge, an accurate description of the post-buckling thermal stresses for plate has not yet been provided.

The present work aims to define a rigorous method to describe the nonlinear thermo-elastic problem for plates employing high-order theories. The governing equations are obtained from the

Principle of Virtual Displacement (PVD), and the nonlinear problem is solved through the Newton-Raphson procedure combined with the arc-length constraint. The plate model is obtained with the Finite Element Method (FEM), and high-order theories are implemented within the CUF framework [31]. The use of CUF presents several advantages; it is based on the building of the Fundamental Nuclei (FN) that makes it possible to write the governing equation in a clear and compact manner for both linear [13] and nonlinear [29] problems. These FNs are the fundamental components of the matrices that describe the structural problem and are independent of the kinematic theory selected. Furthermore, using CUF enables the implementation of a multi-field problem with ease [32].

The paper is organized in the following sections. In Section 2, some preliminary information about FEM and CUF is presented, then in Section 3, the nonlinear equations are developed in terms of FNs, and the solving procedure is described. Section 4 presents the numerical results, and in Section 5, the conclusions are drawn.

2. Refined structural plate models

2.1. Carrera unified formulation and FEM

The problem is schematized considering a plate whose thickness direction is the z-axis of the Cartesian reference system. The unknowns of the problem are the displacement components in the three directions expressed as the displacement vector in Equation (1).

$$\boldsymbol{u}^T(x,y,z) = (u_x, u_y, u_z) \tag{1}$$

These displacement components are expressed through the CUF, which makes it possible to obtain any theory of structures with a generalized kinematic. It is possible to express the unknowns as an arbitrary expansion of the *generalized* displacement through arbitrary thickness functions. The expansion functions are denoted to as F_τ and are functions of the thickness coordinate, the 2D *generalized* displacement are denoted to as $\boldsymbol{u}_\tau$ and depends on the in-plane coordinates. The primary unknowns of the structural problem are expressed in terms of CUF as reported in Equation (2):

$$\boldsymbol{u}(x,y,z) = F_\tau(z)\boldsymbol{u}_\tau(x,y) \qquad \tau = 1,2,...,N \tag{2}$$

where N stands for the number of the terms used in the expansion, and the double subscript denotes summation. The choice of the expansion function and their order of expansion allow one to express any kinematic theory with the same formal notation. Although any thickness function can be used, this paper investigates the use of Lagrange Expansion functions (LE) and Taylor Expansion functions (TE). This choice is justified by previous works, where it is assessed that with these expansion functions, the high-order theories can be implemented with ease as well as the classical plate theories. The adopted expansion theory is denoted by LEn or TEn, where n denotes the order of the expansion.

The LE functions utilize only pure displacement components as primary unknowns; a detailed description and extensive use of Lagrange functions for plate models are described in the literature; examples are [12,33]. Furthermore, these functions are very suitable for layer-wise analyses, see for example [34] describing the influence of the thermo-elastic volumetric strains. TE models are also extensively used in literature for the description of the kinematic theory of the plates [12,33]. These models are based on the calculation of the displacement values on a reference surface, where the displacement along the thickness is described through a polynomial equation whose order denotes the order of expansion. A higher order of expansion can be achieved by adding terms to the displacement field in a hierarchical progression. Classical and high-order

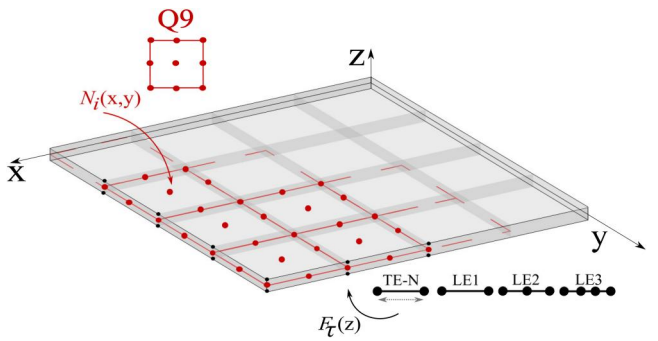


Figure 1. 2D plate models, FEM discretization ad CUF expansion theories.

shear deformation plate theories such as First Order Shear Deformation Theory (FSDT) or Third Order Shear Deformation Theory (TSDT) are examples of TE models, see [31].

Moreover, in the present work, the two models also differ in the description of the material properties along the thickness. TE models characterize stacking sequences using an Equivalent Single Layer (ESL) approach and LE models use a Layer-Wise (LW) model. In the ESL approach, a single expansion is employed describing the whole thickness and as a consequence, the contributes of the different layers to the stiffness matrix are simply added each other. The LW approach considers each ply individually. Interface conditions are enforced by the stiffness matrix assembly, whose dimensions grow with the order of Lagrange expansion and the number of layers. Comprehensive explanations and detailed formulations for both theories can be found in [31].

The FEM is used to discretize the plate within its plane. The 2D unknown vector is written with the combination of the shape functions $N_i(x, y)$ and the nodal displacement vector $\boldsymbol{q}_{\tau i}$ and introducing FEM to the Equation (2) it is possible to explicate the displacement vector as reported in Equation (3). The shape function denotes the type of FEM element that is employed for the in-plane discretization. In the present work nine node bi-quadratic Q9 elements are employed for the FEM discretization.

$$\boldsymbol{u}(x, y, z) = F_\tau(z) N_i(x, y) \boldsymbol{q}_{\tau i} \quad i = 1, 2, ..., M \tag{3}$$

where M denotes the number of nodes adopted in the finite element. The thickness functions and the shape functions are independent each other. As a consequence, M and N can be chosen arbitrarily and mutually independent. A graphical representation of FEM discretization and expansion functions is given in Figure 1.

The explicit form of the vector of nodal displacements is reported in Equation (4).

$$\boldsymbol{q}_{\tau i}^T = \left(q_{x_{\tau i}}, \quad q_{y_{\tau i}}, \quad q_{y_{\tau i}}\right) \tag{4}$$

The use of the present formalism makes it possible to write the following nonlinear equations in a unified way that is applicable to any desired kinematic theory.

2.2. Constitutive and geometrical relations

The strains $\boldsymbol{\varepsilon}$ and the stresses $\boldsymbol{\sigma}$ are written in a general form as in Eqs. (5) and (6), respectively.

$$\boldsymbol{\varepsilon}^T = \left(\varepsilon_{xx}, \varepsilon_{yy}, \varepsilon_{zz}, \varepsilon_{xz}, \varepsilon_{yz}, \varepsilon_{xy}\right) \tag{5}$$

$$\boldsymbol{\sigma}^T = \left(\sigma_{xx}, \sigma_{yy}, \sigma_{zz}, \sigma_{xz}, \sigma_{yz}, \sigma_{xy}\right) \tag{6}$$

The thermo-elastic problem is schematized through a decoupled formulation. This approach means that the displacement field is the only variable of the model, and the thermal profile is

assumed to be known along the whole plate. Furthermore, for the following formulation, the thermal profile is considered constant all over the plate, and the value of the applied overtemperature does not dependent on (x, y, z). As a consequence, it is possible to divide strains and stresses into two components: the pure mechanical and thermal vectors.

$$\boldsymbol{\varepsilon} = \boldsymbol{\varepsilon}_m + \boldsymbol{\varepsilon}_\theta \tag{7}$$

$$\boldsymbol{\sigma} = \boldsymbol{\sigma}_m + \boldsymbol{\sigma}_\theta \tag{8}$$

Here, the subscript m denotes the mechanical part and θ is referred to the thermal component.

The formulation presented in this paper aims to describe the geometrical nonlinear behavior by means of the full 3D Green-Lagrange strain tensor. The pure mechanical strains can be written through the geometrical relations in Eq. (9).

$$\boldsymbol{\varepsilon}_m = \boldsymbol{\varepsilon}_l + \boldsymbol{\varepsilon}_{nl} = (\boldsymbol{b}_l + \boldsymbol{b}_{nl})\boldsymbol{u} \tag{9}$$

In this equation, the geometrical differential operator $\boldsymbol{b}$ is divided into its linear and nonlinear components, which explicit formulation is reported in Eq. (10), where the subscript l is referred to the linear part and nl is for the nonlinear components.

$$\mathbf{b_l} = \begin{pmatrix} \frac{\partial}{\partial x} & 0 & 0 \\ 0 & \frac{\partial}{\partial y} & 0 \\ 0 & 0 & \frac{\partial}{\partial z} \\ \frac{\partial}{\partial z} & 0 & \frac{\partial}{\partial x} \\ 0 & \frac{\partial}{\partial z} & \frac{\partial}{\partial y} \\ \frac{\partial}{\partial y} & \frac{\partial}{\partial x} & 0 \end{pmatrix} \qquad \mathbf{b_{nl}} = \begin{pmatrix} \frac{1}{2}\left(\frac{\partial}{\partial x}\right)^2 & \frac{1}{2}\left(\frac{\partial}{\partial x}\right)^2 & \frac{1}{2}\left(\frac{\partial}{\partial x}\right)^2 \\ \frac{1}{2}\left(\frac{\partial}{\partial y}\right)^2 & \frac{1}{2}\left(\frac{\partial}{\partial y}\right)^2 & \frac{1}{2}\left(\frac{\partial}{\partial y}\right)^2 \\ \frac{1}{2}\left(\frac{\partial}{\partial z}\right)^2 & \frac{1}{2}\left(\frac{\partial}{\partial z}\right)^2 & \frac{1}{2}\left(\frac{\partial}{\partial z}\right)^2 \\ \frac{\partial}{\partial x}\cdot\frac{\partial}{\partial z} & \frac{\partial}{\partial x}\cdot\frac{\partial}{\partial z} & \frac{\partial}{\partial x}\cdot\frac{\partial}{\partial z} \\ \frac{\partial}{\partial y}\cdot\frac{\partial}{\partial z} & \frac{\partial}{\partial y}\cdot\frac{\partial}{\partial z} & \frac{\partial}{\partial y}\cdot\frac{\partial}{\partial z} \\ \frac{\partial}{\partial x}\cdot\frac{\partial}{\partial y} & \frac{\partial}{\partial x}\cdot\frac{\partial}{\partial y} & \frac{\partial}{\partial x}\cdot\frac{\partial}{\partial y} \end{pmatrix} \tag{10}$$

Where the symbol $\partial/\partial(\cdot)$ indicates the partial derivative.

The constitutive equation establishes the strain-stress relation using the global material properties matrix $\boldsymbol{C}$ as reported in Eq. (11). The explicit formulation of the matrix is well known, hereafter it is employed as defined in the Cartesian global reference system and explicit formulation can be found in the literature [31,35].

$$\boldsymbol{\sigma} = \boldsymbol{C}\boldsymbol{\varepsilon} \tag{11}$$

Where the explicit formulation of the elastic matrix $\boldsymbol{C}$ is reported for a generic lamina in Eq. (12).

$$\boldsymbol{C} = \begin{pmatrix} C_{11} & C_{12} & C_{13} & 0 & 0 & C_{16} \\ C_{12} & C_{22} & C_{23} & 0 & 0 & C_{26} \\ C_{13} & C_{23} & C_{33} & 0 & 0 & C_{36} \\ 0 & 0 & 0 & C_{44} & C_{45} & 0 \\ 0 & 0 & 0 & C_{45} & C_{55} & 0 \\ C_{16} & C_{26} & C_{36} & 0 & 0 & C_{66} \end{pmatrix} \tag{12}$$

Strains and stresses are reported in Eq. (13) and Eq. (14) respectively, where the constitutive relations are applied.

$$\boldsymbol{\varepsilon} = \boldsymbol{\varepsilon}_m + \boldsymbol{\varepsilon}_\theta = \boldsymbol{\varepsilon}_m - \boldsymbol{\alpha}\Delta\mathcal{T} = \boldsymbol{\varepsilon}_l + \boldsymbol{\varepsilon}_{nl} - \boldsymbol{\alpha}\Delta\mathcal{T} \tag{13}$$

$$\boldsymbol{\sigma} = \boldsymbol{C}\boldsymbol{\varepsilon} = \boldsymbol{C}(\boldsymbol{\varepsilon}_m + \boldsymbol{\varepsilon}_\theta) = \boldsymbol{C}(\boldsymbol{\varepsilon}_m - \boldsymbol{\alpha}\Delta\mathcal{T}) = \boldsymbol{\sigma}_m - \boldsymbol{\beta}\Delta\mathcal{T} = \boldsymbol{\sigma}_l + \boldsymbol{\sigma}_{nl} + \boldsymbol{\sigma}_\theta \tag{14}$$

Where $\Delta\mathcal{T}$ is the applied overtemperature and $\boldsymbol{\alpha}$ is the vector of the coefficient of thermal expansion whose explicit form is $\boldsymbol{\alpha}^T = (\alpha_1, \alpha_2, \alpha_3, 0, 0, 0)$. $\boldsymbol{\beta}$ couples the thermal and mechanical fields and it is obtained as reported in Eq. (15).

$$\boldsymbol{\beta} = \boldsymbol{C}\boldsymbol{\alpha} = \begin{pmatrix} C_{11} & C_{12} & C_{13} & 0 & 0 & C_{16} \\ C_{12} & C_{22} & C_{23} & 0 & 0 & C_{26} \\ C_{13} & C_{23} & C_{33} & 0 & 0 & C_{36} \\ 0 & 0 & 0 & C_{44} & C_{45} & 0 \\ 0 & 0 & 0 & C_{45} & C_{55} & 0 \\ C_{16} & C_{26} & C_{36} & 0 & 0 & C_{66} \end{pmatrix} \begin{pmatrix} \alpha_1 \\ \alpha_2 \\ \alpha_3 \\ 0 \\ 0 \\ 0 \end{pmatrix} = \begin{pmatrix} \beta_1 \\ \beta_2 \\ \beta_3 \\ 0 \\ 0 \\ \beta_6 \end{pmatrix} \tag{15}$$

where the combination of the thermal expansion coefficients and the material properties matrix create a in-plane shear stress component. Note that the material parameters are considered independent of the temperature. As reported in Eq. (9), the mechanical component of strain and stresses is divided into linear and nonlinear terms. On the other hand, the thermal component is assumed to be linearly dependent on the temperature variation [4,32] and is denoted by the subscript θ.

3. Nonlinear equations of the thermo-elastic equilibrium

Starting from the Principle of Virtual Displacements (PVD), we can impose the following equality between the virtual work of the internal forces δL_{int} and the virtual work of the external load δL_{ext} [36].

$$\delta L_{int} = \delta L_{ext} \tag{16}$$

Assuming that no mechanical external load is applied, the work done by the virtual external load is null, and only the virtual internal work has to be described. Namely one has:

$$\delta L_{int} = \int_V \delta\boldsymbol{\varepsilon}^T \boldsymbol{\sigma} dV = 0 \tag{17}$$

Hereafter, the components of strains defined in Eq. (7) and the constitutive relation from Eq. (11) are substituted inside Eq. (17) to drive the strain energy:

$$\begin{aligned} \delta L_{int} = \int_V \delta\boldsymbol{\varepsilon}^T \boldsymbol{\sigma} dV = \int_V \delta(\boldsymbol{\varepsilon}_m + \boldsymbol{\varepsilon}_\theta)^T \boldsymbol{C}(\boldsymbol{\varepsilon}_m + \boldsymbol{\varepsilon}_\theta) dV = \int_V \delta\boldsymbol{\varepsilon}_m^T \boldsymbol{C}(\boldsymbol{\varepsilon}_m + \boldsymbol{\varepsilon}_\theta) dV \\ + \int_V \cancel{\delta\boldsymbol{\varepsilon}_\theta^T \boldsymbol{C}(\boldsymbol{\varepsilon}_m + \boldsymbol{\varepsilon}_\theta) dV} = \int_V \delta\boldsymbol{\varepsilon}_m^T \boldsymbol{C}\boldsymbol{\varepsilon}_m dV + \int_V \delta\boldsymbol{\varepsilon}_m^T \boldsymbol{C}\boldsymbol{\varepsilon}_\theta dV \end{aligned} \tag{18}$$

where the virtual variation $\delta\boldsymbol{\varepsilon}_\theta$ is null because the thermal strains, described as reported in Eq. (13), do not change with $\boldsymbol{u}$. Furthermore, substituting this definition of thermal strain, the virtual work of the internal forces became as follows:

$$\delta L_{int} = \int_V \delta\boldsymbol{\varepsilon}_m^T \boldsymbol{C}\boldsymbol{\varepsilon}_m dV - \int_V \delta\boldsymbol{\varepsilon}_m^T \boldsymbol{\beta}\Delta\mathcal{T} dV \tag{19}$$

3.1. Derivation of the secant stiffness matrix

From the first term of Eq. (19), it is possible to obtain the secant stiffness matrix $\boldsymbol{K}_s$. Due to the decoupled thermo-elastic approach, the secant stiffness matrix remains unchanged with respect to the pure mechanical problem. Considering that the strains are composed of linear and nonlinear terms it is possible to develop the first part of Eq. (19) as reported below.

$$\begin{aligned}\int_V \delta\boldsymbol{\varepsilon}_m^T \boldsymbol{C}\boldsymbol{\varepsilon}_m dV &= \int_V \delta(\boldsymbol{\varepsilon}_l + \boldsymbol{\varepsilon}_{nl})^T \boldsymbol{C}(\boldsymbol{\varepsilon}_l + \boldsymbol{\varepsilon}_{nl}) dV \\ &= \int_V \delta\boldsymbol{\varepsilon}_l^T \boldsymbol{C}\boldsymbol{\varepsilon}_l dV + \int_V \delta\boldsymbol{\varepsilon}_l^T \boldsymbol{C}\boldsymbol{\varepsilon}_{nl} dV + \int_V \delta\boldsymbol{\varepsilon}_{nl}^T \boldsymbol{C}\boldsymbol{\varepsilon}_l dV + \int_V \delta\boldsymbol{\varepsilon}_{nl}^T \boldsymbol{C}\boldsymbol{\varepsilon}_{nl} dV\end{aligned} \tag{20}$$

Substituting CUF and FEM from Eq. (3), it is possible to obtain the following formulation:

$$\begin{aligned}\int_V \delta\boldsymbol{\varepsilon}_m^T \boldsymbol{C}\boldsymbol{\varepsilon}_m dV = &\int_V \delta\Big(\boldsymbol{b}_l F_s(z) N_j(x,y)\boldsymbol{q}_{sj}\Big)^T \boldsymbol{C}\big(\boldsymbol{b}_l F_\tau(z) N_i(x,y)\boldsymbol{q}_{\tau i}\big) dV \\ &+ \int_V \delta\Big(\boldsymbol{b}_l F_s(z) N_j(x,y)\boldsymbol{q}_{sj}\Big)^T \boldsymbol{C}\big(\boldsymbol{b}_{nl} F_\tau(z) N_i(x,y)\boldsymbol{q}_{\tau i}\big) dV \\ &+ \int_V \delta\Big(\boldsymbol{b}_{nl} F_s(z) N_j(x,y)\boldsymbol{q}_{sj}\Big)^T \boldsymbol{C}\big(\boldsymbol{b}_l F_\tau(z) N_i(x,y)\boldsymbol{q}_{\tau i}\big) dV \\ &+ \int_V \delta\Big(\boldsymbol{b}_{nl} F_s(z) N_j(x,y)\boldsymbol{q}_{sj}\Big)^T \boldsymbol{C}\big(\boldsymbol{b}_{nl} F_\tau(z) N_i(x,y)\boldsymbol{q}_{\tau i}\big) dV\end{aligned} \tag{21}$$

where the application of the differential operator $\boldsymbol{b}$ on the expansion and shape functions allows us to obtain the matrices $\boldsymbol{B}_l$ and $\boldsymbol{B}_{nl}$. The FNs of these matrices are $\boldsymbol{B}_l^{\tau i}$ and $\boldsymbol{B}_{nl}^{\tau i}$ whose explicit formulations are reported in Eqs. (22) and (23):

$$\boldsymbol{B}_l^{\tau i} = \boldsymbol{b}_l\big(F_\tau(z) N_i(x,y)\big) = \begin{bmatrix} F_\tau N_{i,x} & 0 & 0 \\ 0 & F_\tau N_{i,y} & 0 \\ 0 & 0 & F_{\tau,z} N_i \\ F_{\tau,z} N_i & 0 & F_\tau N_{i,x} \\ 0 & F_{\tau,z} N_i & F_\tau N_{i,y} \\ F_\tau N_{i,y} & F_\tau N_{i,x} & 0 \end{bmatrix} \tag{22}$$

$$\boldsymbol{B}_{nl}^{\tau i} = \boldsymbol{b}_{nl}\big(F_\tau(z) N_i(x,y)\big) = \frac{1}{2}\begin{bmatrix} u_{x,x} F_\tau N_{i,x} & u_{y,x} F_\tau N_{i,x} & u_{z,x} F_\tau N_{i,x} \\ u_{x,y} F_\tau N_{i,y} & u_{y,y} F_\tau N_{i,y} & u_{z,y} F_\tau N_{i,y} \\ u_{x,z} F_{\tau,z} N_i & u_{y,z} F_{\tau,z} N_i & u_{z,z} F_{\tau,z} N_i \\ u_{x,x} F_{\tau,z} N_i + u_{x,z} F_\tau N_{i,x} & u_{y,x} F_{\tau,z} N_i + u_{y,z} F_\tau N_{i,x} & u_{z,x} F_{\tau,z} N_i + u_{z,z} F_\tau N_{i,x} \\ u_{x,y} F_{\tau,z} N_i + u_{x,z} F_\tau N_{i,y} & u_{y,y} F_{\tau,z} N_i + u_{y,z} F_\tau N_{i,y} & u_{z,y} F_{\tau,z} N_i + u_{z,z} F_\tau N_{i,y} \\ u_{x,x} F_\tau N_{i,y} + u_{x,y} F_\tau N_{i,x} & u_{y,x} F_\tau N_{i,y} + u_{y,y} F_\tau N_{i,x} & u_{z,x} F_\tau N_{i,y} + u_{z,y} F_\tau N_{i,x} \end{bmatrix} \tag{23}$$

where the subscript ',' stands for the derivative. In Eq. (21) it is necessary to calculate the virtual variation $\delta(\boldsymbol{B}_l^{sj}\boldsymbol{q}_{sj})$ and $\delta(\boldsymbol{B}_{nl}^{sj}\boldsymbol{q}_{sj})$. Due to the linearity of the matrix $\boldsymbol{B}_l$ the differential operator δ acts only on $\boldsymbol{q}_{sj}$ and the application of the virtual variation results in $\boldsymbol{B}_l^{sj}\delta\boldsymbol{q}_{sj}$. Different is the case of $\boldsymbol{B}_{nl}$, which is dependent on the unknown of the problem as outlined in Eq. (23). It is possible to demonstrate that $\delta(\boldsymbol{B}_{nl}^{sj}\boldsymbol{q}_{sj}) = 2\boldsymbol{B}_{nl}^{sj}\delta\boldsymbol{q}_{sj}$. Note that, for the definition of the FNs and the assembly procedure that follows, F_τ and N_i are referred to the physical quantities while, when the virtual variation is applied, the indices are *sj*. However, the matrices with apexes *sj* and τi are formally the same.

Applying the virtual variation, Eq. (21) becomes as follows:

$$\begin{aligned}\int_V \delta\boldsymbol{\varepsilon}_m^T \boldsymbol{C}\boldsymbol{\varepsilon}_m dV &= \int_V \delta\boldsymbol{q}_{sj}^T \boldsymbol{B}_l^{sjT} \boldsymbol{C}\boldsymbol{B}_l^{\tau i}\boldsymbol{q}_{\tau i} dV + \int_V \delta\boldsymbol{q}_{sj}^T \boldsymbol{B}_l^{sjT} \boldsymbol{C}\boldsymbol{B}_{nl}^{\tau i}\boldsymbol{q}_{\tau i} dV \\ &\quad + \int_V \delta\boldsymbol{q}_{sj}^T 2\boldsymbol{B}_{nl}^{sjT} \boldsymbol{C}\boldsymbol{B}_l^{\tau i}\boldsymbol{q}_{\tau i} dV + \int_V \delta\boldsymbol{q}_{sj}^T 2\boldsymbol{B}_{nl}^{sjT} \boldsymbol{C}\boldsymbol{B}_{nl}^{\tau i}\boldsymbol{q}_{\tau i} dV \\ &= \delta\boldsymbol{q}_{sj}^T \Big[\boldsymbol{K}_0^{ij\tau s} + \boldsymbol{K}_{lnl}^{ij\tau s} + \boldsymbol{K}_{nll}^{ij\tau s} + \boldsymbol{K}_{nlnl}^{ij\tau s}\Big]\boldsymbol{q}_{\tau i}\end{aligned} \tag{24}$$

Equation (24) reports the components of the secant stiffness matrix where $\boldsymbol{K}_0^{ij\tau s}$ is the linear component of $\boldsymbol{K}_s$, and it is coincident to the linear stiffness matrix. $\boldsymbol{K}_{lnl}^{ij\tau s}$ and $\boldsymbol{K}_{nll}^{ij\tau s}$ are the nonlinear terms of the first order and $\boldsymbol{K}_{nlnl}^{ij\tau s}$ is the second order nonlinear component. All the

components of the matrices are well known and are not reported in explicit form hereafter but can be found in the literature [29]. It is relevant to note that the matrix $\boldsymbol{K}_s$ is not symmetric. However there are available procedures to express it in a symmetric form, see [37].

3.2. Derivation of the thermal load vector

From the second part of Eq. (19), it is possible to obtain the vector of the thermal load $\boldsymbol{F}_\theta$ following what is written in Eq. (25).

$$\begin{aligned}\int_V \delta\boldsymbol{\varepsilon}_m^T\boldsymbol{\beta}\Delta\mathcal{T}\,dV &= \int_V \delta\left(\boldsymbol{\varepsilon}_l^T+\boldsymbol{\varepsilon}_{nl}^T\right)\boldsymbol{\beta}\Delta\mathcal{T}\,dV = \int_V \delta\boldsymbol{\varepsilon}_l^T\boldsymbol{\beta}\Delta\mathcal{T}\,dV + \int_V \delta\boldsymbol{\varepsilon}_{nl}^T\boldsymbol{\beta}\Delta\mathcal{T}\,dV \\ &= \int_V \delta\left(\boldsymbol{b}_l F_s(z)N_j(x,y)\boldsymbol{q}_{sj}\right)^T\boldsymbol{\beta}\Delta\mathcal{T}\,dV + \int_V \delta\left(\boldsymbol{b}_{nl} F_s(z)N_j(x,y)\boldsymbol{q}_{sj}\right)^T\boldsymbol{\beta}\Delta\mathcal{T}\,dV\end{aligned} \tag{25}$$

Substituting Eqs. (22) and (23) into Eq. (25), and using the differential operator as reported in Section 3.1, it is possible to obtain the following expression.

$$\begin{aligned}\int_V \delta\boldsymbol{q}_{sj}^T\boldsymbol{B}_l^{sjT}\boldsymbol{\beta}\Delta\mathcal{T}\,dV + 2\int_V \delta\boldsymbol{q}_{sj}^T\boldsymbol{B}_{nl}^{sjT}\boldsymbol{\beta}\Delta\mathcal{T}\,dV &= \delta\boldsymbol{q}_{sj}^T\left[\int_V \boldsymbol{B}_l^{sjT}\boldsymbol{\beta}\Delta\mathcal{T}\,dV + \int_V 2\boldsymbol{B}_{nl}^{sjT}\boldsymbol{\beta}\Delta\mathcal{T}\,dV\right] \\ &= \delta\boldsymbol{q}_{sj}^T\left[\boldsymbol{F}_{\theta_l}^{sj}+\boldsymbol{F}_{\theta_{nl}}^{sj}\right]\end{aligned} \tag{26}$$

For the sake of clarity, the linear and nonlinear terms of the load vector are divided into two different components. Due to the nature of the thermal load, a nonlinear part of the load vector arises.

From Eq. (26), it is possible to obtain the components of the FNs of the linear and nonlinear thermal vectors as reported in Eqs. (27) and (28), respectively.

$$\boldsymbol{F}_{\theta_l}^{sj} = \left\{\begin{array}{l}\Delta\mathcal{T}\int_V\left[\beta_1 F_s N_{j,x}+\beta_6 F_s N_{j,y}\right]dV \\ \Delta\mathcal{T}\int_V\left[\beta_2 F_s N_{j,y}+\beta_6 F_s N_{j,x}\right]dV \\ \Delta\mathcal{T}\int_V \beta_3 F_{s,z} N_j dV\end{array}\right\} \tag{27}$$

$$\boldsymbol{F}_{\theta_{nl}}^{sj} = \left\{\begin{array}{l}\Delta\mathcal{T}\int_V\left[\beta_1 u_{x,x}F_s N_{j,x}+\beta_2 u_{x,y}F_s N_{j,y}+\beta_3 u_{x,z}F_{s,z}N_j+\beta_6(u_{x,x}F_s N_{j,y}+u_{x,y}F_s N_{j,x})\right]dV \\ \Delta\mathcal{T}\int_V\left[\beta_1 u_{y,x}F_s N_{j,x}+\beta_2 u_{y,y}F_s N_{j,y}+\beta_3 u_{y,z}F_{s,z}N_j+\beta_6(u_{y,x}F_s N_{j,y}+u_{y,y}F_s N_{j,x})\right]dV \\ \Delta\mathcal{T}\int_V\left[\beta_1 u_{z,x}F_s N_{j,x}+\beta_2 u_{z,y}F_s N_{j,y}+\beta_3 u_{z,z}F_{s,z}N_j+\beta_6(u_{z,x}F_s N_{j,y}+u_{z,y}F_s N_{j,x})\right]dV\end{array}\right\} \tag{28}$$

It is possible to note that there is a linear relationship between the overtemperature and the load vector, and the nonlinear part of the problem is dependent on the displacement gradient.

Starting from the PVD and adding what is obtained in Eqs. (24) and (26), the governing equation described in terms of FN can be written as in Eq. (29):

$$\begin{aligned}\delta L_{int} &= \int_V \delta\boldsymbol{\varepsilon}^T\boldsymbol{\sigma}dV = \int_V \delta\boldsymbol{\varepsilon}_m^T\boldsymbol{C}\boldsymbol{\varepsilon}_m dV - \int_V \delta\boldsymbol{\varepsilon}_m^T\boldsymbol{\beta}\Delta\mathcal{T}\,dV \\ &= \delta\boldsymbol{q}_{sj}^T\left[\boldsymbol{K}_0^{ij\tau s}+\boldsymbol{K}_{lnl}^{ij\tau s}+\boldsymbol{K}_{nll}^{ij\tau s}+\boldsymbol{K}_{nlnl}^{ij\tau s}\right]\boldsymbol{q}_{\tau i} - \delta\boldsymbol{q}_{sj}^T\left[\boldsymbol{F}_{\theta_l}^{sj}+\boldsymbol{F}_{\theta_{nl}}^{sj}\right] = 0\end{aligned} \tag{29}$$

that in a compact form is rewritten as:

$$\delta \boldsymbol{q}_{sj}: \quad \boldsymbol{K}_s^{ij\tau s}\boldsymbol{q}_{\tau i} - \boldsymbol{F}_\theta^{sj} = 0 \tag{30}$$

The governing equation is written in terms of FN which are the basic components of each matrix or vector that describe the problem. They consists of 3×3 matrix or 3×1 vector whose form does not change depending on the adopted theory as well as on the number of DOF. The equation, expressed in terms of FNs, pertains to a single layer k of the plate. It can be assembled in accordance with the Equivalent-Single-Layer (ESL) or Layer-Wise (LW) model as detailed in [31].

Starting from the equations written in terms of FN and proceeding with assembly, it is possible to obtain all the vectors and matrices of each structural problem. The assembly procedure is a trivial operation that consist of four loops acting on four indices. The indices of the procedure are denoted here as τ, i, s, j referring to the corresponding expansion and shape function. Indices s, j are relative to the virtual variation and τ, i denotes the physical quantities. Details about the FNs and the assembly procedure are described by Carrera et al. [31].

Through the assembly procedure it is possible to rewrite Eq. (30) as follows:

$$\boldsymbol{K}_s\boldsymbol{q} - \boldsymbol{F}_\theta = 0 \tag{31}$$

Equation (31) describes a nonlinear set of equations that can not be solved directly, and, as a consequence, it is necessary to introduce an incremental linearized scheme. In order to use the Newton-Raphson method [38], one can define the residual nodal force vector as:

$$\boldsymbol{\varphi}_{res} = \boldsymbol{K}_S\boldsymbol{q} - \boldsymbol{F}_\theta \tag{32}$$

To solve the problem, it is necessary to minimize the residual nodal forces vector since, at the equilibrium, the residual is null.

3.3. Newton-Raphson

Starting from Eq. (32), it is possible to linearize the equation, expanding it in Taylor's series about the known solution $(\boldsymbol{q}, \Delta T)$. Considering only the first-order terms of the expansion, Eq. (32) is written as:

$$\boldsymbol{\varphi}_{res}(\boldsymbol{q} + \delta\boldsymbol{q}, \Delta\mathcal{T} + \delta\Delta\mathcal{T}) = \boldsymbol{\varphi}_{res}(\boldsymbol{q}, \Delta\mathcal{T}) + \left.\frac{\partial \boldsymbol{\varphi}_{res}}{\partial \boldsymbol{q}}\right|_{\boldsymbol{q}} \delta\boldsymbol{q} + \left.\frac{\partial \boldsymbol{\varphi}_{res}}{\partial(\Delta\mathcal{T})}\right|_{\Delta\mathcal{T}} \delta\lambda(\Delta\mathcal{T})_{ref} = 0 \tag{33}$$

In Eq. (33) it is assumed that the thermal load varies directly with the initial thermal loading $(\Delta\mathcal{T})_{ref}$ with a rate of change λ.

It is possible to define a stiffness matrix called *tangent stiffness matrix* $\boldsymbol{K}_T = \frac{\partial \boldsymbol{\varphi}_{res}}{\partial \boldsymbol{q}}|_{\boldsymbol{q}}$ and a new thermal load vector called *tangent thermal load vector* $\tilde{\boldsymbol{F}}_\theta = -\frac{\partial \boldsymbol{\varphi}_{res}}{\partial(\Delta\mathcal{T})}|_{\Delta\mathcal{T}}(\Delta\mathcal{T})_{ref}$. For the sake of simplicity, this last vector is split into linear and nonlinear parts. Substituting the definitions of the matrix and the new vector, the Taylor's expansion written in Eq. (33) becomes as follows.

$$\boldsymbol{\varphi}_{res}(\boldsymbol{q} + \delta\boldsymbol{q}, \Delta\mathcal{T} + \delta\Delta\mathcal{T}) = \boldsymbol{\varphi}_{res}(\boldsymbol{q}, \Delta\mathcal{T}) + \boldsymbol{K}_T\delta\boldsymbol{q} - (\tilde{\boldsymbol{F}}_{\theta_l} + \tilde{\boldsymbol{F}}_{\theta_{nl}})\delta\lambda = 0 \tag{34}$$

Equation (34) can be written as:

$$\boldsymbol{K}_T\delta\boldsymbol{q} = \tilde{\boldsymbol{F}}_\theta\delta\lambda - \boldsymbol{\varphi}_{res}(\boldsymbol{q}, \Delta\mathcal{T}) \tag{35}$$

In these equations, the loading scaling parameter λ is introduced in the problem as a variable of the equation system. As a consequence, it is necessary to couple Eq. (35) with a general constraint equation to close the problem. The obtained system can be written as follows:

$$\begin{cases} \boldsymbol{K}_T \delta \boldsymbol{q} = \tilde{\boldsymbol{F}}_\theta \delta\lambda - \boldsymbol{\varphi}_{res} \\ \boldsymbol{c}(\delta \boldsymbol{q}, \delta\lambda) = 0 \end{cases} \tag{36}$$

The choice of the constraint equation defines the incremental scheme that will be followed in the numerical solution procedure. Depending on the constraint, it is possible to define, for instance, the load control method with the relationship $\delta\lambda = 0$, the displacement control method with $\delta \boldsymbol{q} = 0$ and the path following method acting on both $\delta\lambda$ and $\delta \boldsymbol{q}$.

In the present work, the path-following method introduced by Crisfield [39] and later modified by Carrera [40] is adopted. The implementation of this method in combination with CUF is detailed in [37], and several applications have been published, see for example [29]. The adopted constraint corresponds to a multi-dimensional sphere whose radius length is equal to the arch-length value. The radius starts at the initial arch length denoted as L_0 and changes at each load step. Furthermore, here, the *full* Newton-Raphson method is employed, and the tangent matrix as well as the load vector are updated at each iteration considering the new unknown values.

3.4. Derivation of the tangent stiffness matrix

Equation (37) reports the definition of the tangent stiffness matrix reporting the linearization of the virtual strain energy:

$$\delta^2 L_{int} = \delta \boldsymbol{q}_{sj}^T \boldsymbol{K}_T^{ij\tau s} \delta \boldsymbol{q}_{\tau i} \tag{37}$$

Starting from the definition of internal virtual work in Eq. (17), the application of the virtual variation results into Eq. (38):

$$\delta^2 L_{int} = \delta\left(\int_V \delta \boldsymbol{\varepsilon}_m^T \boldsymbol{\sigma} dV \right) = \int_V \delta \boldsymbol{\varepsilon}_m^T \delta \boldsymbol{\sigma} dV + \int_V \delta^2 \boldsymbol{\varepsilon}_m^T \boldsymbol{\sigma} dV \tag{38}$$

In order to obtain the full tangent stiffness matrix, it is worthwhile to develop each component of the equation separate and define the different matrices that compose the tangent matrix. The first term of Eq. (38) demands the linearization of the constitutive equations (14). It is assumed that the material properties do not depend on the unknown $\boldsymbol{q}$; as a consequence, the derivative operator acts on the strain part of the constitutive equations. The relation can be developed as follows:

$$\begin{aligned} \int_V \delta \boldsymbol{\varepsilon}_m^T \delta \boldsymbol{\sigma} dV &= \int_V \delta \boldsymbol{\varepsilon}_m^T \delta(\boldsymbol{\sigma}_m + \boldsymbol{\sigma}_\theta) dV = \int_V \delta \boldsymbol{\varepsilon}_m^T \delta \boldsymbol{\sigma}_m dV + \int_V \delta \boldsymbol{\varepsilon}_m^T \delta \boldsymbol{\sigma}_\theta dV \\ &= \int_V \delta(\boldsymbol{\varepsilon}_l + \boldsymbol{\varepsilon}_{nl})^T \delta(\boldsymbol{\sigma}_l + \boldsymbol{\sigma}_{nl}) dV = \int_V \delta(\boldsymbol{\varepsilon}_l + \boldsymbol{\varepsilon}_{nl})^T \boldsymbol{C} \delta(\boldsymbol{\varepsilon}_l + \boldsymbol{\varepsilon}_{nl}) dV \\ &= \int_V \delta \boldsymbol{\varepsilon}_l^T \boldsymbol{C} \delta \boldsymbol{\varepsilon}_l dV + \int_V \delta \boldsymbol{\varepsilon}_{nl}^T \boldsymbol{C} \delta \boldsymbol{\varepsilon}_l dV + \int_V \delta \boldsymbol{\varepsilon}_l^T \boldsymbol{C} \delta \boldsymbol{\varepsilon}_{nl} dV + \int_V \delta \boldsymbol{\varepsilon}_{nl}^T \boldsymbol{C} \delta \boldsymbol{\varepsilon}_{nl} dV \end{aligned} \tag{39}$$

In Eq. (39) the variational operator applied on the thermal stress give us a null component due to the definition of the thermal stress ($\boldsymbol{\sigma}_\theta = -\beta \Delta \mathcal{T}$). Moreover, the material properties are assumed as constant, and the virtual variation applied on the stresses does not affect the $\boldsymbol{C}$ matrix.

Substituting Eqs. (9) and (11) in Eq. (39) and considering the derivative rules, it is possible to define the components of the tangent matrix described in the first part of Eq. (38) in terms of FNs.

$$\int_V \delta \boldsymbol{\varepsilon}_l^T \boldsymbol{C} \delta \boldsymbol{\varepsilon}_l dV = \delta \boldsymbol{q}_{s\tau}^T \int_V \boldsymbol{B}_l^{sjT} \boldsymbol{C} \boldsymbol{B}_l^{\tau i} dV \delta \boldsymbol{q}^{\tau i} = \delta \boldsymbol{q}_{sj}^T \boldsymbol{K}_0^{ij\tau s} \delta \boldsymbol{q}_{\tau i} \tag{40}$$

$$\int_V \delta\boldsymbol{\varepsilon}_{nl}^T \boldsymbol{C}\delta\boldsymbol{\varepsilon}_l dV = \delta\boldsymbol{q}_{s\tau}^T \int_V 2\boldsymbol{B}_{nl}^{sjT}\boldsymbol{C}\boldsymbol{B}_l^{\tau i} dV \delta\boldsymbol{q}^{\tau i} = \delta\boldsymbol{q}_{sj}^T \boldsymbol{K}_{nll}^{ij\tau s}\delta\boldsymbol{q}_{\tau i} \tag{41}$$

$$\int_V \delta\boldsymbol{\varepsilon}_l^T \boldsymbol{C}\delta\boldsymbol{\varepsilon}_{nl} dV = \delta\boldsymbol{q}_{s\tau}^T \int_V \boldsymbol{B}_l^{sjT}\boldsymbol{C}2\boldsymbol{B}_{nl}^{\tau i} dV \delta\boldsymbol{q}^{\tau i} = \delta\boldsymbol{q}_{sj}^T 2\boldsymbol{K}_{lnl}^{ij\tau s}\delta\boldsymbol{q}_{\tau i} \tag{42}$$

$$\int_V \delta\boldsymbol{\varepsilon}_{nl}^T \boldsymbol{C}\delta\boldsymbol{\varepsilon}_{nl} dV = \delta\boldsymbol{q}_{s\tau}^T \int_V 2\boldsymbol{B}_{nl}^{sjT}\boldsymbol{C}2\boldsymbol{B}_{nl}^{\tau i} dV \delta\boldsymbol{q}^{\tau i} = \delta\boldsymbol{q}_{sj}^T 2\boldsymbol{K}_{nlnl}^{ij\tau s}\delta\boldsymbol{q}_{\tau i} \tag{43}$$

As a consequence, Eq. (39) becomes as follows:

$$\int_V \delta\boldsymbol{\varepsilon}_m^T \delta\boldsymbol{\sigma} dV = \delta\boldsymbol{q}_{sj}^T \left[\boldsymbol{K}_0^{ij\tau s} + \boldsymbol{K}_{nll}^{ij\tau s} + 2\boldsymbol{K}_{lnl}^{ij\tau s} + 2\boldsymbol{K}_{nlnl}^{ij\tau s}\right]\delta\boldsymbol{q}_{\tau i} = \delta\boldsymbol{q}_{sj}^T \left[\boldsymbol{K}_0^{ij\tau s} + \boldsymbol{K}_{T1}^{ij\tau s}\right]\delta\boldsymbol{q}_{\tau i} \tag{44}$$

$\boldsymbol{K}_{T1}^{ij\tau s}$ is the nonlinear contribution of the tangent stiffness matrix. However, the FNs described in Eqs. (40)–(43) coincide with the FNs of the secant stiffness matrix reported in Section 3.1. Moreover, it should be noted that, unlike the secant stiffness matrix, the tangent stiffness matrix is symmetric.

The second part of Eq. (38) is developed in Eq. (45).

$$\int_V \delta^2\boldsymbol{\varepsilon}_m^T \boldsymbol{\sigma} dV = \int_V \not{\delta}^2\boldsymbol{\varepsilon}_l{}^T \boldsymbol{\sigma} dV + \int_V \delta^2\boldsymbol{\varepsilon}_{nl}^T \boldsymbol{\sigma} dV \tag{45}$$

where the second variation on the linear part of the strain vector in null.

The application of the second-order variation and the explicit formulation of the second variation of strains are not here reported but can be find in [37].

With some simple manipulations, it is possible to express $\delta^2\boldsymbol{\varepsilon}_{nl}$ vector as the combination of the matrix $\boldsymbol{B}_{nl}^*$ and a vector with the product of the virtual variations of nodal unknowns as expressed in Eq. (46). The explicit formulation of matrix $\boldsymbol{B}_{nl}^*$ is given in Appendix A.

$$\delta^2\boldsymbol{\varepsilon}_{nl} = \boldsymbol{B}_{nl}^* \begin{Bmatrix} \delta q_{x_{\tau i}}\delta q_{x_{sj}} \\ \delta q_{y_{\tau i}}\delta q_{y_{sj}} \\ \delta q_{z_{\tau i}}\delta q_{z_{sj}} \end{Bmatrix} \tag{46}$$

Equation (45) can now be developed as follows:

$$\int_V \delta^2\boldsymbol{\varepsilon}_{nl}^T \boldsymbol{\sigma} dV = \int_V \left(\boldsymbol{B}_{nl}^* \begin{Bmatrix} \delta q_{x_{\tau i}}\delta q_{x_{sj}} \\ \delta q_{y_{\tau i}}\delta q_{y_{sj}} \\ \delta q_{z_{\tau i}}\delta q_{z_{sj}} \end{Bmatrix}\right)^T \boldsymbol{\sigma} dV = \int_V \left(\boldsymbol{B}_{nl}^* \begin{Bmatrix} \delta q_{x_{\tau i}}\delta q_{x_{sj}} \\ \delta q_{y_{\tau i}}\delta q_{y_{sj}} \\ \delta q_{z_{\tau i}}\delta q_{z_{sj}} \end{Bmatrix}\right)^T (\boldsymbol{\sigma}_l + \boldsymbol{\sigma}_{nl} + \boldsymbol{\sigma}_\theta) dV =$$
$$\delta\boldsymbol{q}_{sj}^T \int_V diag(\boldsymbol{B}_{nl}^{*T}(\boldsymbol{\sigma}_l + \boldsymbol{\sigma}_{nl} + \boldsymbol{\sigma}_\theta)) dV \delta\boldsymbol{q}_{\tau i} = \delta\boldsymbol{q}_{sj}^T \left[\boldsymbol{K}_{\sigma l}^{ij\tau s} + \boldsymbol{K}_{\sigma nl}^{ij\tau s} + \boldsymbol{K}_{\sigma\theta}^{ij\tau s}\right]\delta\boldsymbol{q}_{\tau i} = \delta\boldsymbol{q}_{sj}^T \left[\boldsymbol{K}_{\sigma}^{ij\tau s} + \boldsymbol{K}_{\sigma\theta}^{ij\tau s}\right]\delta\boldsymbol{q}_{\tau i} \tag{47}$$

The first two matrices $\boldsymbol{K}_{\sigma l}$ and $\boldsymbol{K}_{\sigma nl}$ are the geometrical matrices which depend on pure mechanical stress and, can be found in literature [29]. The last matrix collects the thermal components and his explicit formulation is reported in Eq. (48).

$$\boldsymbol{K}_{\sigma\theta}^{ij\tau s} = -\Delta\mathcal{T}(\beta_1 \int_h F_\tau F_s dz \int_\Omega N_{i,x} N_{j,x} dA + \beta_2 \int_h F_\tau F_s dz \int_\Omega N_{i,y} N_{j,y} dA + \beta_3 \int_h F_{\tau,z} F_{s,z} dz \int_\Omega N_i N_j dA$$
$$+ \beta_6 \int_h F_\tau F_s dz \int_\Omega N_{i,x} N_{j,y} dA + \beta_6 \int_h F_\tau F_s dz \int_\Omega N_{i,y} N_{j,x} dA)\boldsymbol{I} \tag{48}$$

Where $\boldsymbol{I}$ denotes the 3×3 identity matrix, $dA = dxdy$, Ω is the reference surface and h is the thickness.

All the terms of Eq. (38) are here written in terms of 3×3 FNs. The summation of the components reported in Eq. (44) and Eq. (47) allow us to obtain the FNs of the complete tangent stiffness matrix as reported follows:

$$\begin{aligned}\delta \boldsymbol{q}_{sj}^T \boldsymbol{K}_T^{ij\tau s} \delta \boldsymbol{q}_{\tau i} &= \int_V \delta \boldsymbol{\varepsilon}_m^T \delta \boldsymbol{\sigma} dV + \int_V \delta^2 \boldsymbol{\varepsilon}_m^T \boldsymbol{\sigma} dV \\ &= \delta \boldsymbol{q}_{sj}^T \left[\boldsymbol{K}_0^{ij\tau s} + \boldsymbol{K}_{T1}^{ij\tau s} \right] \delta \boldsymbol{q}_{\tau i} + \delta \boldsymbol{q}_{sj}^T \left[\boldsymbol{K}_{\sigma 0}^{ij\tau s} + \boldsymbol{K}_{\sigma nl}^{ij\tau s} + \boldsymbol{K}_{\sigma \theta}^{ij\tau s} \right] \delta \boldsymbol{q}_{\tau i} \\ &= \delta \boldsymbol{q}_{sj}^T \left[\boldsymbol{K}_0^{ij\tau s} + \boldsymbol{K}_{T1}^{ij\tau s} + \boldsymbol{K}_{\sigma 0}^{ij\tau s} + \boldsymbol{K}_{\sigma nl}^{ij\tau s} + \boldsymbol{K}_{\sigma \theta}^{ij\tau s} \right] \delta \boldsymbol{q}_{\tau i}\end{aligned} \tag{49}$$

3.5. Derivation of the tangent load vector

Writing the governing equation in Taylor's series as reported in Eq. (33) allows us to obtain a new vector defined as $\tilde{\boldsymbol{F}}_\theta = -\frac{\partial \boldsymbol{\varphi}_{res}}{\partial(\Delta \mathcal{T})}\Big|_{\Delta \mathcal{T}} (\Delta \mathcal{T})_{ref}$. Applying this definition, it is possible to write the FN of this vector from Eq. (50).

$$\tilde{\boldsymbol{F}}_\theta = -\frac{\partial (\boldsymbol{K}_s \boldsymbol{q} - \boldsymbol{F}_\theta)}{\partial \Delta \mathcal{T}}\Big|_{\Delta \mathcal{T}} (\Delta \mathcal{T})_{ref} = \frac{\partial (\boldsymbol{F}_\theta)}{\partial \Delta \mathcal{T}}\Big|_{\Delta \mathcal{T}} (\Delta \mathcal{T})_{ref} \tag{50}$$

Starting from the definition of the FN of the thermal load vector reported in Section 3.2, it is easy to obtain the tangent vector nuclei as reported in Eqs. (51) and (52) where, for the sake of clarity, linear and nonlinear terms are split into two vectors.

$$\tilde{\boldsymbol{F}}_{\theta_l}^{sj} = (\Delta \mathcal{T})_{ref} \cdot \begin{Bmatrix} \int_V \left[\beta_1 F_s N_{j,x} + \beta_6 F_s N_{j,y} \right] dV \\ \int_V \left[\beta_2 F_s N_{j,y} + \beta_6 F_s N_{j,x} \right] dV \\ \int_V \beta_3 F_{s,z} N_j dV \end{Bmatrix} \tag{51}$$

$$\tilde{\boldsymbol{F}}_{\theta_{nl}}^{sj} = (\Delta \mathcal{T})_{ref} \cdot \begin{Bmatrix} \int_V \left[\beta_1 u_{x,x} F_s N_{j,x} + \beta_2 u_{x,y} F_s N_{j,y} + \beta_3 u_{x,z} F_{s,z} N_j + \beta_6 (u_{x,x} F_s N_{j,y} + u_{x,y} F_s N_{j,x}) \right] dV \\ \int_V \left[\beta_1 u_{y,x} F_s N_{j,x} + \beta_2 u_{y,y} F_s N_{j,y} + \beta_3 u_{y,z} F_{s,z} N_j + \beta_6 (u_{y,x} F_s N_{j,y} + u_{y,y} F_s N_{j,x}) \right] dV \\ \int_V \left[\beta_1 u_{z,x} F_s N_{j,x} + \beta_2 u_{z,y} F_s N_{j,y} + \beta_3 u_{z,z} F_{s,z} N_j + \beta_6 (u_{z,x} F_s N_{j,y} + u_{z,y} F_s N_{j,x}) \right] dV \end{Bmatrix} \tag{52}$$

It is important to consider this additional term in the description of the nonlinear thermal problem. The nonlinear component expressed in Eq. (52) is dependent on the displacement value. As a consequence, the choice of the path following constraint that allows us to act on both load and displacement parameters is advisable for a good convergence trend.

4. Numerical results

In the following section, analyses are presented which compare the present method with results in the literature. Furthermore, some results regarding the stresses developed along the plate are reported, comparing pre-buckling and post-buckling conditions. It is assumed that the temperature profile is known and constant throughout the plate.

In the current section, the adopted expansion theory is denoted by LEn or TEn for the Lagrange and Taylor models, respectively, where n denotes the order of the expansion. For each

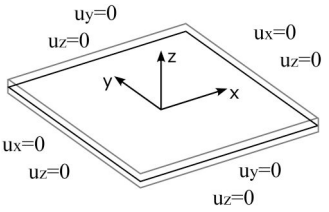


Figure 2. Representation of the simply supported constraints. All the constraints are applied on the Middle surface.

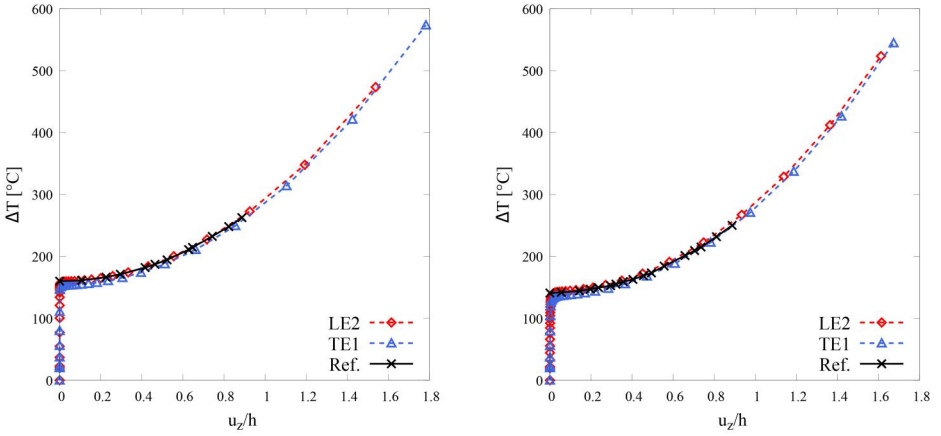


Figure 3. $E_1 = 400GPa, E_2 = E_3 = 10GPa, G = 5GPa, \nu = 0.25, \alpha = 1 \times 10^{-6} 1/^{\circ}C$, Mesh 10×10 Q9, present models compared to [26], (a) $[-45/45]_6$, (b) $[-30/30]_6$.

analysis the adopted model is indicated, and when LE is employed, it is understood to be relative to the individual layer of the plate. That is to say that a model with mLEn uses a number of m LE elements of order n for each layer. The FEM in-plane discretization is conducted employing nine-node quad elements, denoted as Q9.

Attention is focused on the capabilities of the present method to describe the 3D thermal stress in a large equilibrium regime, evaluating also the influence of shear and volumetric effect on the 3D deformation state.

4.1. Verification

In the present subsection, some verification analyses are reported comparing the results with Chen et al. [26]. The evaluation point is situated at the center of the plate, and the constraint is simply supported, as illustrated in Figure 2. With this constraint, the edges are fixed against normal displacements; however, they can translate in the tangential direction.

For $z = 0, x = \pm L/2$: $u_x = 0 \quad u_z = 0$,

For $z = 0, y = \pm L/2$: $u_y = 0 \quad u_z = 0$.

Figures 3a and 3b show analyses conducted on a square plate made of a laminate composed of orthotropic material. The results are compared to the one obtained by Chen et al. [26]. The material properties are $E_1 = 400GPa, E_2 = E_3 = 10GPa, G = 5GPa, \nu = 0.25, \alpha = 1 \times 10^{-6} 1/^{\circ}C$. The dimensions of the plate are $L = 1m$, thickness of $h = 10mm$. Two laminations are considered: $[-45/45]_6$, and $[-30/30]_6$. After a convergence analysis, a 10×10 Q9 mesh is chosen. $TE1$ and $LE2$ models are chosen to compare the high-order LW model to a linear model with ESL multilayer modelization.

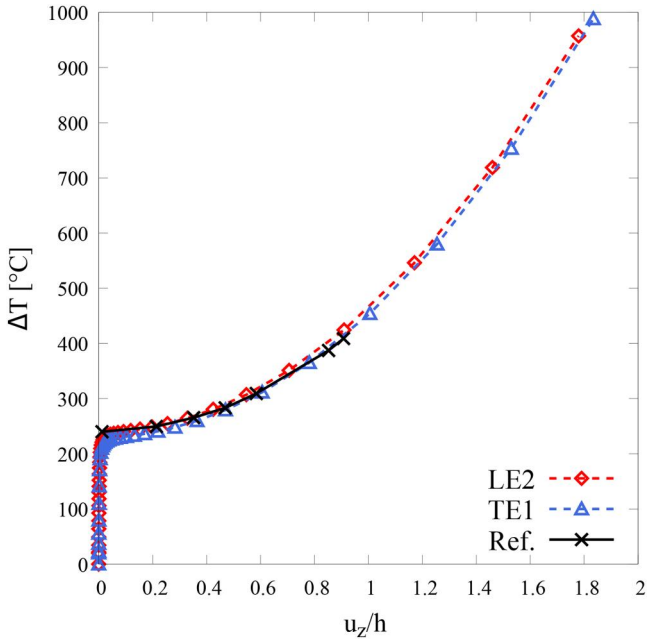


Figure 4. Rectangular plate $a/b = 1.5$, $E_1 = 400GPa, E_2 = E_3 = 10GPa, G = 5GPa, \nu = 0.25, \alpha = 1x10^{-6}1/^{\circ}C$, lamination of $[-45/45]_6$, mesh 10 × 5 Q9, present models compared to [26].

From Figure 3, it is clear that the buckling critical temperature is equal to $160^{\circ}C$ for the 45° lamination and $144^{\circ}C$ for the 30° lamination. The nondimensional displacement coincides with the reference for each analysis conducted. The reference, reported in the graphs, is calculated only for low levels of nonlinearities; on the other hand, the present method reaches higher values of the overtemperature.

Figure 4 reports the results of an analysis conducted on a rectangular plate made by the same material of the previous case with a lamination of $[-45/45]_6$ and a change in the dimension of one edge, making the ratio $a/b = 1.5$.

Also, in the case of rectangular shape, the results are comparable to the reference without notable differences.

4.2. Displacement and stresses results

Hereafter, a model presented by Meyers et al. [28] is analyzed where a higher temperature is reached.

The plate is square shaped with edges 150 mm long, the total thickness is 1.016 mm, and the material properties are $E_1 = 155GPa, E_2 = E_3 = 8.07GPa, \nu = 0.22, G_{12} = G_{13} = G_{23}4.55GPa, \alpha_1 = -0.07 \times 10^{-6}1/^{\circ}C, \alpha_2 = \alpha_3 = 30.1 \times 10^{-6}1/^{\circ}C$. The plate is simply supported on all the edges as reported in Figure 2.

Figures 5a and 5b report the displacement in the z-axis direction obtained through the present method compared to the reference one and the one obtained with a Nastran 2D model which comprises 10 × 10 Q4 plate elements.

After a convergence analysis on the displacement, a mesh of 10 × 10 Q9 is chosen for the present model. The analyzed laminations are $[45/-45/0/90]_s$ and $[45/-45/0/0]_s$, where the first is a nearly-isotropic lamination. Due to the symmetry of the plates in terms of lamination and temperature distribution, an imperfection that guarantees buckling is obtained by inserting a defect in the lamination with a 2-degree change to the third layer orientation.

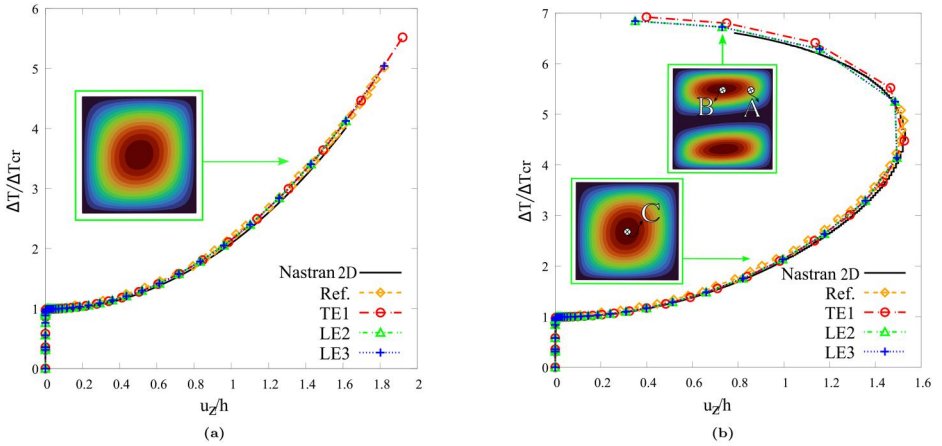


Figure 5. Dimensionless u_z displacement for square shaped plate with simply supported constraint as reported in Figure 2, present models compared to [28]. Two different laminations: (a) $[45/-45/0/90]_s$, (b) $[45/-45/0/0]_s$. Subfig. (b) reports Point C in the center of the plate (0,0,0), Point A ($L/4$, $L/4$, 0) and Point B (0, $L/4$,0).

As illustrated in Figure 5, the non-dimensional z-axis displacement, denoted as u_z/h, is presented in comparison to the non-dimensional over-temperature, indicated as $\Delta T/\Delta T_{cr}$. Furthermore, the post-buckling shape is depicted in the figures.

Due to the chosen laminations, the linearized buckling temperature is the same for both plates, and it is $\Delta T_{cr} = 38.6^{\circ}C$. The linearized buckling temperature is obtained using an eigenvalue procedure; details can be found in [34]. For this analysis a $20 \times 20Q9$ Discretization with expansion theory LE2 is chosen for each layer. The displacement is taken in Point C at the center of the plate, which coincides with the maximum displacement for the nearly-isotropic lamination. The displacement reported in Figure 5b is the central displacement, which coincides with the maximum displacement only until a change of shape is reached. An increase in the applied temperature leads to an abrupt change in buckled shape, which results in a *secondary buckling*. As a consequence, an increase in the applied temperature results in a lower displacement in the center of the plate, and the maximum displacement for the higher level of nonlinearities is located at another point. This phenomenon can occur in a structure that is already in a post-buckling regime. When the applied over-temperature increases, a sudden change in the equilibrium path can be observed. It corresponds to a variation in the deformed configuration, which may exhibit a change in the number of *half-waves* in the x and y directions. This deformation should not be interpreted as the activation of a higher-order linear buckling mode. However, it consists of a nonlinear instability developed along the post-buckling equilibrium path. Further information can be found, for example, in [41].

The temperature reached in the reported analysis is approximately $270^{\circ}C$. At such elevated temperatures, a change in material properties is to be expected. However, it is not considered in this study.

Some results in terms of stress distribution are proposed below. Therefore, a second convergence analysis is conducted on the stresses to ensure an accurate evaluation. This analysis is performed on the $[45/-45/0/0]_s$ plate, which exhibits higher anisotropy and slower convergence than the nearly isotropic plate. The results of this analysis are reported in Figures 6, 7, and 8, where three different conditions of thermal load are considered. After the convergence analysis a mesh of 20 × 20 Q9 elements is chosen.

Figure 6 reports the convergence analysis on stresses conducted in a pre-buckling condition. The applied overtemperature is $\Delta T = 12^{\circ}C$. The out-of-plane stresses are not reported because

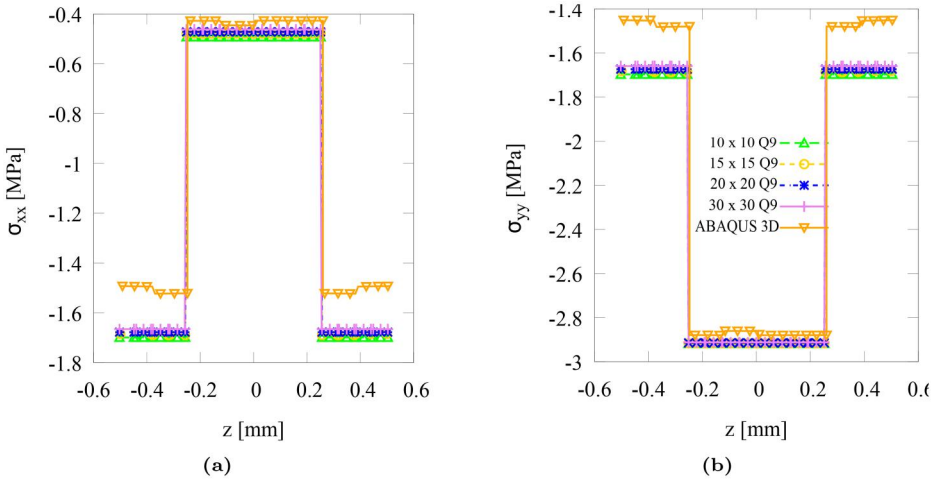


Figure 6. Convergence analysis changing the number of Q9 elements on square plate with $[45/-45/0/0]_s$ lamination. (a) σ_{xx}, (b) σ_{yy}. LE2 expansion, results taken in Point C, $\Delta T = 12^{\circ}C$.

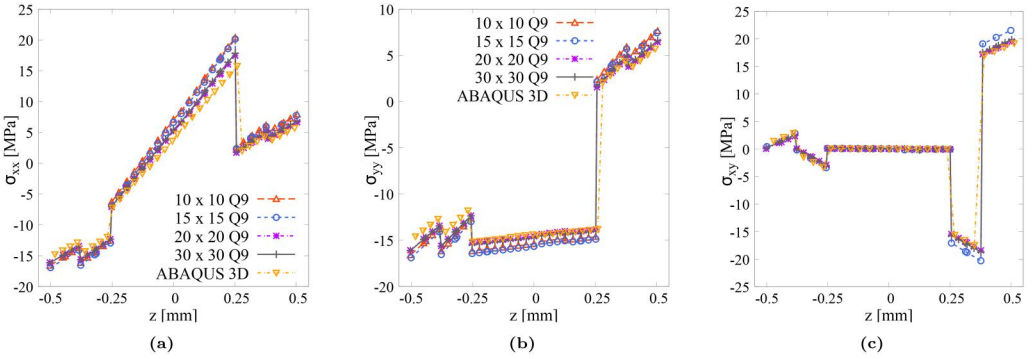


Figure 7. Convergence analysis changing the number of Q9 elements on square plate with $[45/-45/0/0]_s$ lamination. (a) σ_{xx}, (b) σ_{yy}, (c) σ_{xy}. LE2 expansion, results taken in Point C, $\Delta T = 60^{\circ}C$.

they are null. Figure 7 reports the convergence analysis on the stress in the post-buckling configuration at $\Delta T = 60^{\circ}C$, and Figure 8 collects the convergence in the *secondary buckling* at $\Delta T = 260^{\circ}C$.

As clear from Figures 7 and 8, the description of stresses requires a denser mesh than in the case of displacement. When the convergence analysis is carried out on the post-buckling results, the discretization requires to ensure good results becomes higher than the one necessary for the pre-buckling condition. Furthermore, it is clear from the results in Figure 7, that the in-plane stresses can also be considered correct even for a coarse mesh. However, the out-of-plane stresses require a dense mesh to ensure good results. As the temperature increases, the difference in these results increases. For the configuration analyzed in Figure 8 also for the in-plane stresses, there is a clear difference between 15 × 15 and 20 × 20 Q9 meshes. These results clearly show that the optimum convergence mesh is different between the pre-buckling and post-buckling configurations. The post-buckling convergence mesh is chosen to ensure good results throughout the analysis from lower to higher loading conditions. Furthermore, the convergence analysis here reported helps to ensure that in the present study there is no visible shear locking. This is guaranteed by using the correct number of elements combined with the shape functions polynomial order (bi-quadratic elements), further details about locking can be find in [42]. After the convergence analysis, the expansion theory is also changed to compare the various stress results

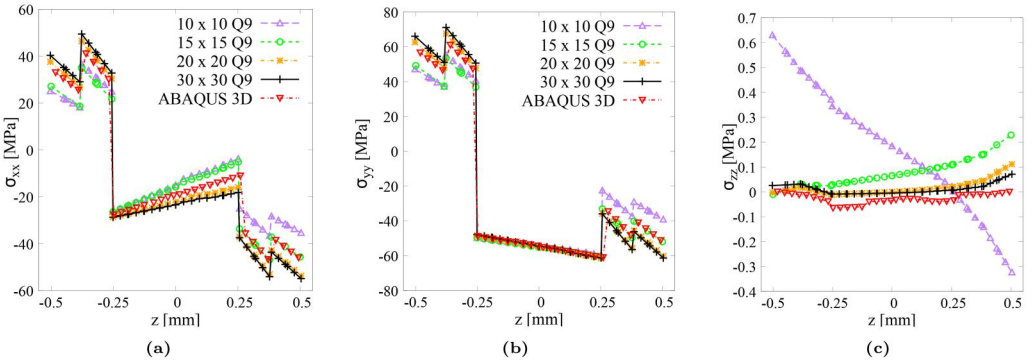


Figure 8. Convergence analysis changing the number of Q9 elements on square plate with $[45/-45/0/0]_s$ lamination. (a) σ_{xx}, (b) σ_{yy}, (c) σ_{zz}. LE2 expansion, results taken in Point C, $\Delta T = 260^{\circ}C$.

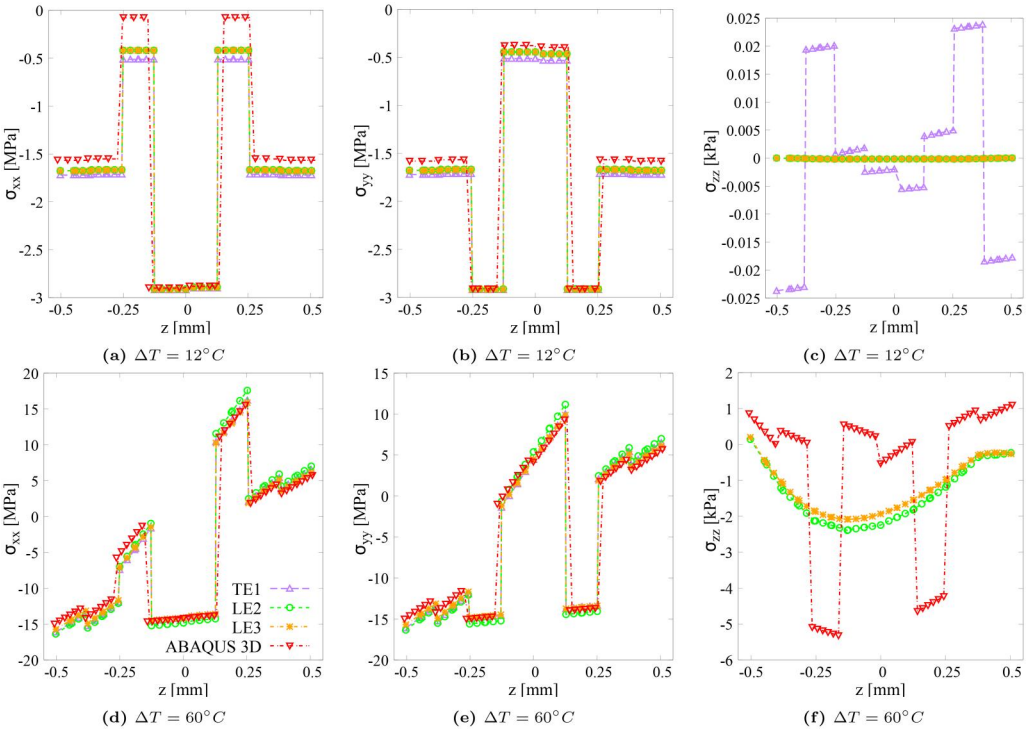


Figure 9. Stress of square shaped plate with simply supported constraint and lamination $[45/-45/0/90]_s$. results taken in Point C, comparing pre-buckling results with $\Delta T = 12^{\circ}C$ and post-buckling stresses for $\Delta T = 60^{\circ}C$. Pre buckling results in (a) σ_{xx}, (b) σ_{yy}, (c) σ_{zz} and post-buckling stresses in (d) σ_{xx}, (e) σ_{yy}, (f) σ_{zz}. Comparison of the stress results for *LE* and *TE* with 20 × 20 Q9 mesh.

obtained through TE and LE models. Figure 9, shows stresses obtained along the nearly-isotropic plate which has a lamination of $[45/-45/90/0]_s$. The results are taken in the center of the plate for both the pre-buckling configuration with $\Delta T = 12^{\circ}C$ and post-buckling condition with $\Delta T = 60^{\circ}C$. The same results are collected in Table 1 where the stresses are taken in Point C with $z = 0.128$ mm.

From Figure 9 and Table 1, it is evident that the stresses obtained in the post-buckling condition are higher in magnitude than in the pre-buckling condition due to the greater intensity of the load. However, this trend of stress is not directly linked only to the load; rather, it is

Table 1. Stress and displacement of square shaped plate with simply supported constraint and lamination $[45/-45/0/90]_s$.

Theory	u_z [mm]	σ_{xx} [MPa]	σ_{zz} [MPa]	σ_{yz} [MPa]	DOFs
$\Delta T = 12^\circ C$					
TE1	0.6143×10^{-4}	−1.0177	−1.8798	-0.6118×10^{-6}	11094
LE2	0.6151×10^{-4}	−1.0004	−1.8792	-0.2255×10^{-6}	94299
LE3	0.6151×10^{-4}	−1.0004	−1.8792	-0.2255×10^{-6}	138875
$\Delta T = 60^\circ C$					
TE1	0.7313	11.2808	0.1619	0.9992×10^{-2}	11094
LE2	0.7296	11.2201	0.3101×10^{-2}	0.9548×10^{-2}	94299
LE3	0.7296	11.2131	0.3266×10^{-2}	0.9453×10^{-2}	138875

Results taken in point C at $z = 0.128$ mm.

Table 2. Stress and displacement of square plate with simply supported constraint and lamination $[45/-45/0/0]_s$.

Theory	u_z [mm]	σ_{xx} [MPa]	σ_{yy} [MPa]	u_z [mm]	σ_{xx} [MPa]	σ_{yy} [MPa]	DOFs
	Point B			Point C			
$\Delta T = 60^\circ C$							
TE1	0.5457	6.4968	−14.3112	0.6907	11.9689	−14.3638	11094
LE2	0.5317	6.2732	−14.1508	0.6717	11.4535	−14.2015	94299
LE3	0.5317	6.1678	−14.0401	0.6717	11.3726	−14.0121	138875
$\Delta T = 260^\circ C$							
TE1	1.3862	21.1004	−50.8784	0.7408	−28.4250	−58.9978	11094
LE2	1.4793	27.5127	−51.8907	0.7416	−27.8075	−58.0474	94299
LE3	1.4793	27.0468	−51.2521	0.7416	−26.7292	−62.0445	138875

Results taken in point B and point C at $z = 0.128$ mm.

indicative of a different trend from the classic case of linear behavior with low levels of displacement. This difference is more evident from the Table 2, where it is clear from the various values of stresses that a non linear relation describes the plate behavior. Furthermore, the observed lack of symmetry in the post-buckling results can attributed to the deflection that occurs in the buckled condition, with the stresses effectively representing a bending condition. This is a condition that is not present in the pre-buckling configuration, where the plate remains flat until it reaches the buckling load.

The shear stress σ_{yz} is zero for the pre-buckling condition and change for the post-buckling state; the value at the edge of the plate is not zero due to the nonlinear behavior, as demonstrated in [43].

As clear from the Table 1, the stress through the thickness σ_{zz} is not well captured through the *TE*1 model, whose value is not reported in the graph because it is two orders of magnitude higher than the value obtained through the *LE* models.

Figures 10 and 11 and Tables 2 and 3 report the stresses for the analysis of the plate with $[45/-45/0/0]_s$ lamination, for $\Delta T = 60^\circ C$ and $\Delta T = 260^\circ C$. The in-plane normal stresses are reported in Figure 10 comparing the results in Point C and Point B using different expansion theories.

As illustrated in Figure 10, a comparison is made between the in-plane stresses σ_{xx} and σ_{yy} at Point C and Point B, for the two buckled configuration under consideration. The results are reported for the two specific values of applied overtemperature whose choice was thus defined by the presence of the maximum u_z displacement at Point C for the $\Delta T = 60C^\circ$ and at Point B for the $\Delta T = 260^\circ C$.

When the plate is deflected as the first buckled mode, the two points exhibit approximately equivalent values for both the reported stresses σ_{xx} and σ_{yy}. Conversely, in the *secondary buckling* configuration, the trend is opposite for the two points, indicating the two distinct directions of deflection. The use of different kinematic models does not affect the results of the in-plane normal stresses. A divergent scenario emerges when out-of-plane stresses are taken into consideration, as demonstrated in Figure 9, where it is evident that the *TE*1 models are inadequate in

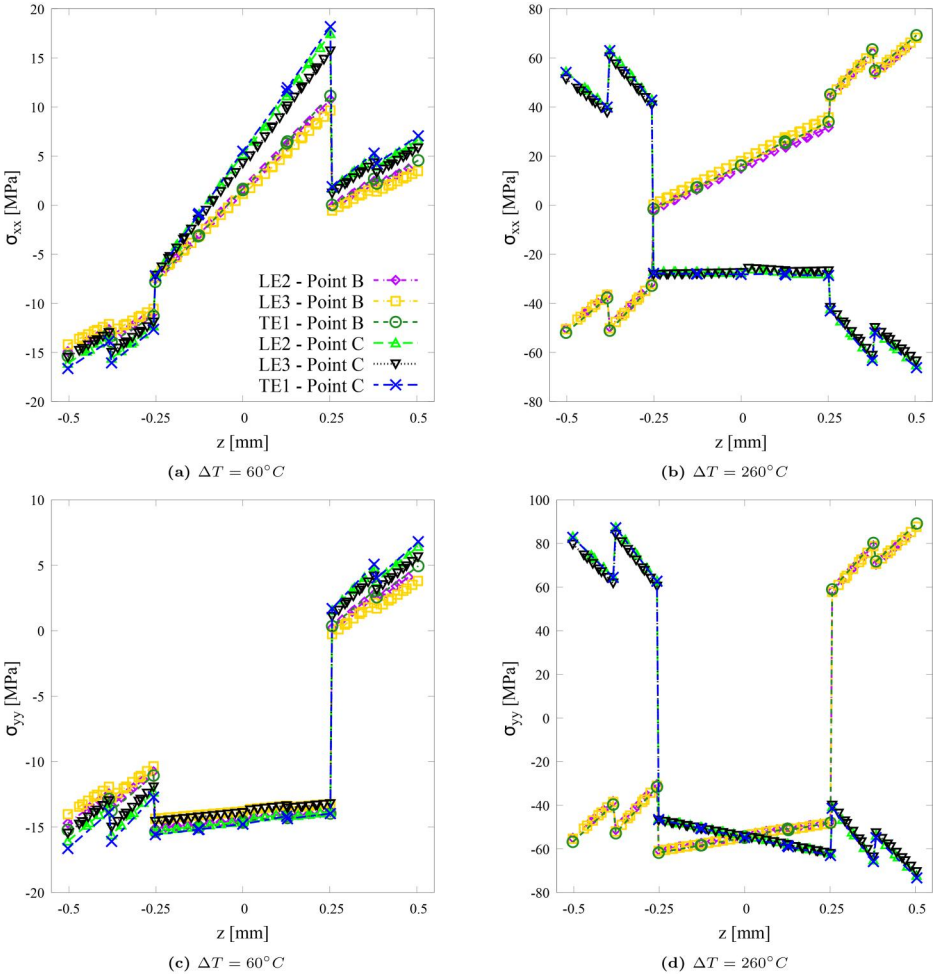


Figure 10. In-Plane normal stress σ_{xx} (a), (b), and σ_{yy} (c), (d) for simply supported square shaped plate with $[45/-45/0/0]_s$ lamination. Results taken in Point C and Point B for two different overtemperatures, 20 × 20 Q9.

describing the trend of the out-of-plane stresses. As a consequence, Figure 11 reports $\sigma_{zz}, \sigma_{xz}, \sigma_{yz}$ without considering *TE*1 model. The reported results are compared for the three evaluation points, whose coordinates are reported in Figure 5.

In accordance with the prevailing expectations, the stresses reported in Figure 11 are consistent with the continuity conditions at the interface of the layers. The results of σ_{zz} are presented for all three evaluation points. Again, an inverted trend is observed at Points C and S for the post-buckling condition, as previously reported in Figure 10. When reporting the results of σ_{xz} and σ_{yz}, it is noted that the values at Point C have not been included as they are negligible.

4.3. Cantilever plate

Hereafter, a different case study is reported. A rectangular plate composed of two layers of isotropic material is considered. The plate dimensions are $a = 1m, b = 0.5m, t = 10mm$. The first layer of the laminate is composed of aluminum, whose properties are $E = 73MPa, \nu = 0.33, \alpha = 25 \times 10^{-6} 1/^{\circ}C$. The second layer is made of steel, whose properties are: $E = 210MPa, \nu =$

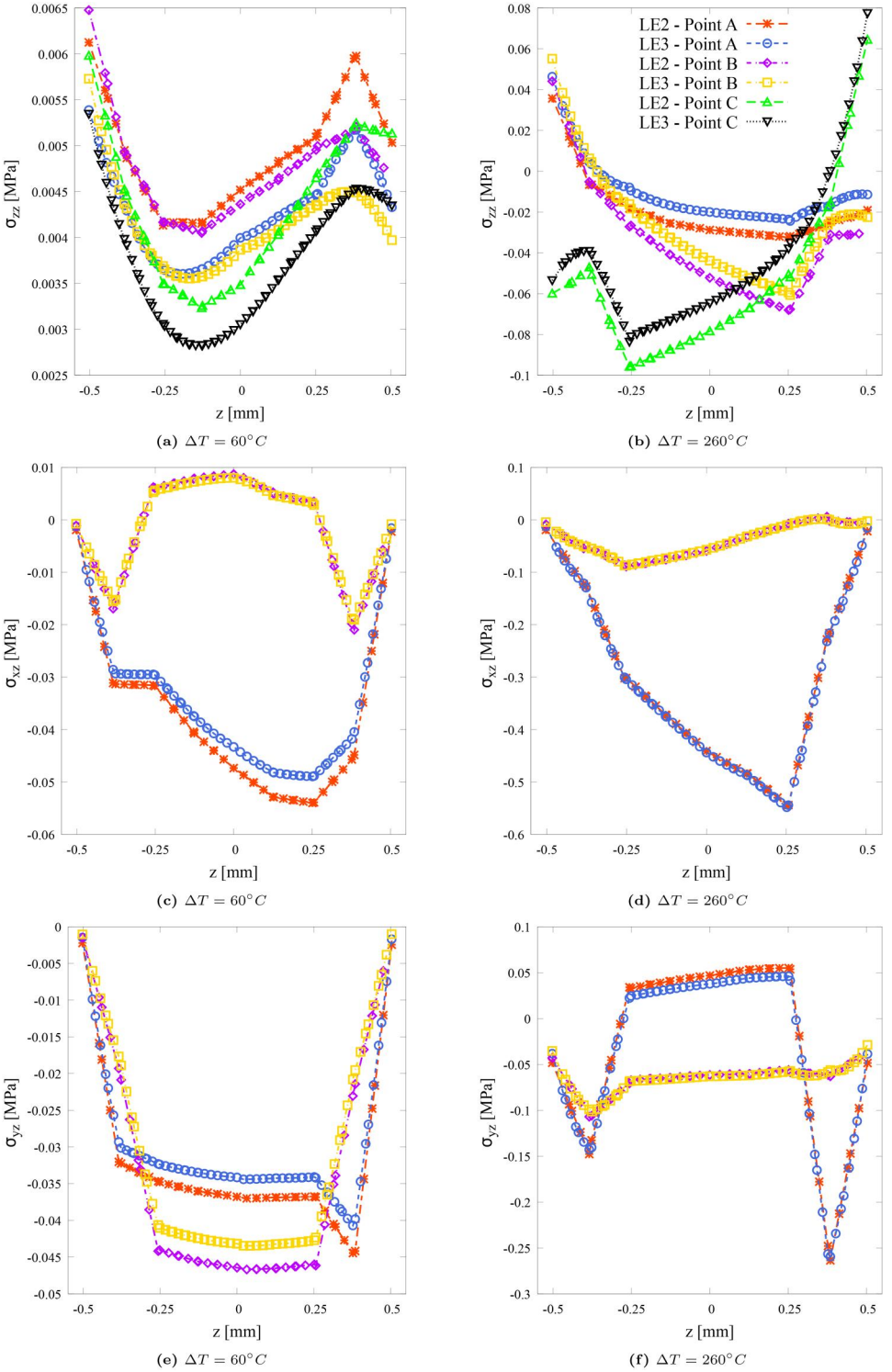


Figure 11. Out-of-plane stresses (a), (b) σ_{zz}, (c), (d) σ_{xz}, (e), (f) σ_{yz}. simply supported square shaped plate with $[45/-45/0/0]_s$ lamination. Results taken in Point C, Point B and point a for two different overtemperatures, 20 × 20 Q9.

Table 3. Stress of square shaped plate with simply supported constraint and lamination $[45/-45/0/0]_s$.

Theory	σ_{zz} [MPa]	σ_{xz} [MPa]	σ_{yz} [MPa]	σ_{zz} [MPa]	σ_{xz} [MPa]	σ_{yz} [MPa]	DOFs
	Point B			Point A			
$\Delta\mathcal{T} = 60^{\circ}C$							
LE2	0.4651×10^{-2}	0.4910×10^{-2}	-0.4651×10^{-1}	0.4833×10^{-2}	-0.5287×10^{-1}	-0.3688×10^{-1}	94299
LE3	0.4288×10^{-2}	0.4684×10^{-2}	-0.4322×10^{-1}	0.4232×10^{-2}	-0.6703×10^{-1}	-0.4416×10^{-1}	138875
$\Delta\mathcal{T} = 260^{\circ}C$							
LE2	-0.6080×10^{-1}	-0.3170×10^{-1}	-0.6055×10^{-1}	-0.3051×10^{-1}	-0.4835	0.5302×10^{-1}	94299
LE3	-0.5242×10^{-1}	-0.3138×10^{-1}	-0.6197×10^{-1}	-0.2198×10^{-1}	-0.4873	0.4410×10^{-1}	138875

Results taken in point B and point C at $z = 0.128$ mm.

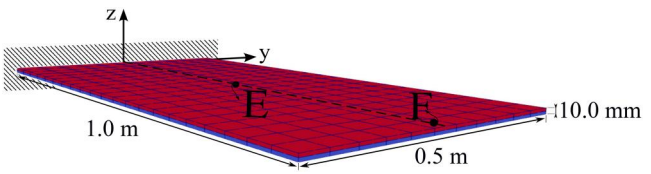


Figure 12. Geometry of the bimetallic plate. Bottom layer composed of aluminum, top layer made of steel. Point E ($a/2$, 0, 0), Point F (a, 0, 0).

$0.2, \alpha = 12\times10^{-6}1/^{\circ}C$. The plate is clamped along one of the shorter edges as reported in Figure 12. In this case study, the focus is not on the post-buckling phenomenon, as in the previous sections, but rather on the study of high displacement resulting from an increase in thermal load. Indeed, the plate is constrained only on one edge, and there are no conditions for the buckling phenomena.

Figure 13 compares the non-dimensional displacement in z-axis and x-axis direction obtained though the present method with a mesh of 20×10 Q9 and the Nastran 2D results, which are obtained with a 12×6 Q4 discretization. Different expansion functions are employed, and a linear analysis is conducted to evaluate the importance of the nonlinear analysis. The results are taken in Point E and Point F, whose coordinates are reported in Figure 12.

The present analysis is focused on large displacements; however, as is evident in the graphs, a nonlinear analysis is also necessary at lower loads. Furthermore, the displacement results indicate that no buckling phenomena occur; nevertheless, due to the high deflection, a nonlinear analysis is also mandatory. The displacement in the thickness direction also follows a linear trend at high temperatures, whilst the displacement in the x-axis direction is highly nonlinear. When u_x is calculated through a linear analysis, it reports a displacement direction opposite to the true one. This linear analysis describes only the expansion of the material, ignoring the bending and the high displacement and rotations that cannot be captured through a linear analysis.

The *TE*1 model is the only one that leads to inaccurate results, and the displacement is already accurately represented by the *TE*2 model.

In order to describe the rise stresses, Figure 14 reports the stresses trend for a convergence analysis. Other analyses with lower elements mesh were conducted, but they are too far from the good results to be reported.

From the results in Figure 14, a mesh of 33×15 Q9 is chosen to ensure good results with a lower computational cost. The in-plane normal results are not affected by the number of elements; instead, the out-of-plane results drive the choice of discretization.

Figure 15 and Table 4 report the stresses obtained with different expansion theories. The TE models cannot provide good results for the σ_{zz}, and to have a clear representation, they are not reported in the figure. Due to the considered materials and geometry, σ_{yz} is negligible and is not reported.

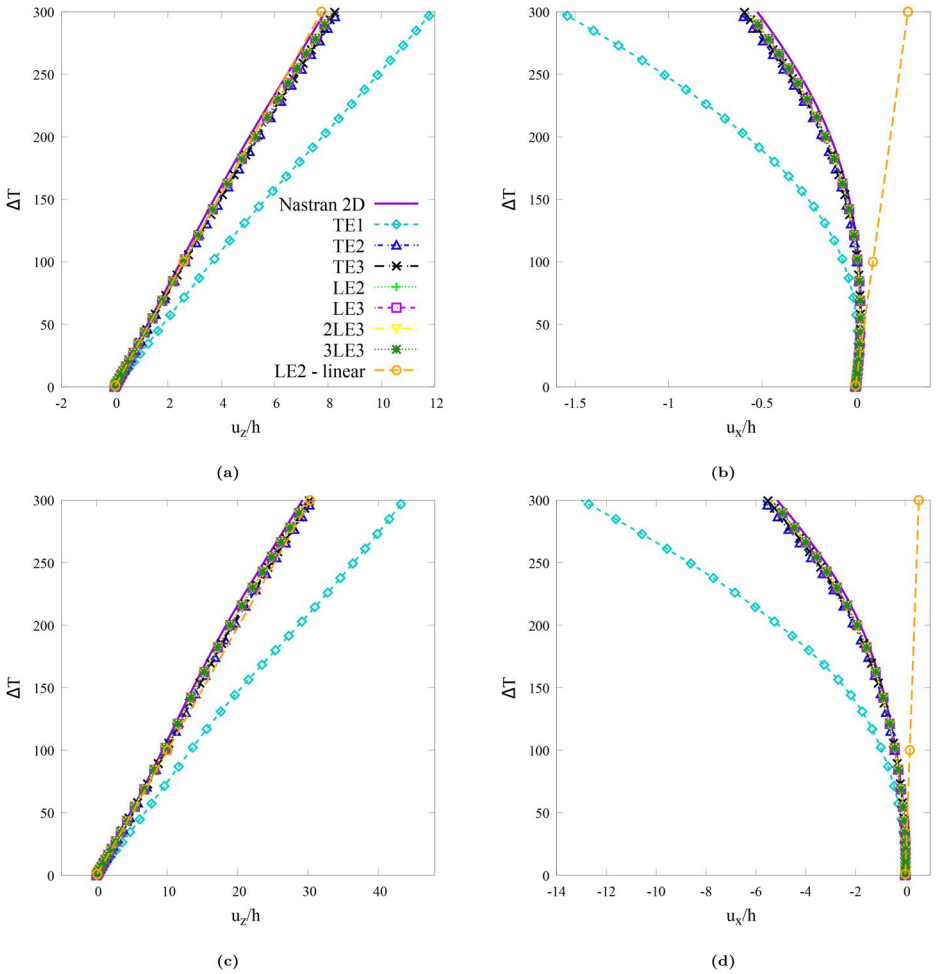


Figure 13. Laminate cantilever plate composed of aluminum and steel, present method 20 × 10 Q9, Nastran 2D 12 × 6 Q4. (a), (b) Point E, (c), (d) Point F.

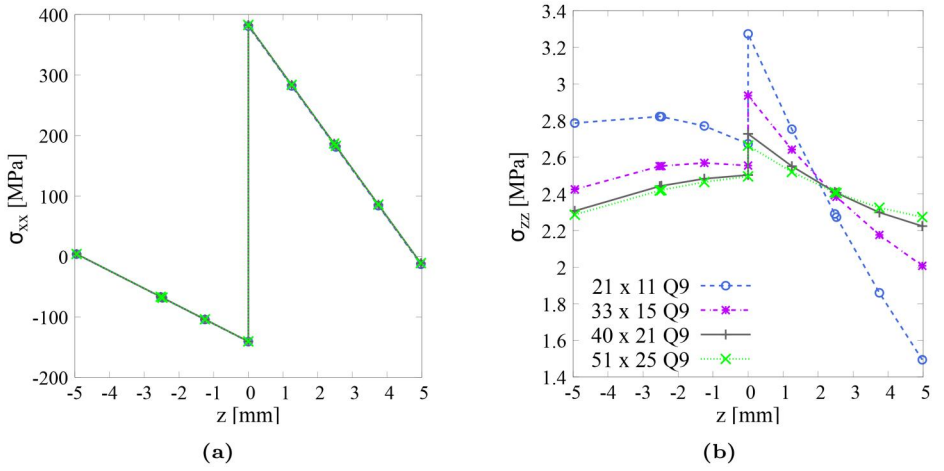


Figure 14. Bimetallic cantilever plate, convergence analysis on stresses, changing the number of Q9 elements. Results taken in point E with $\Delta T = 200^{\circ} C$.

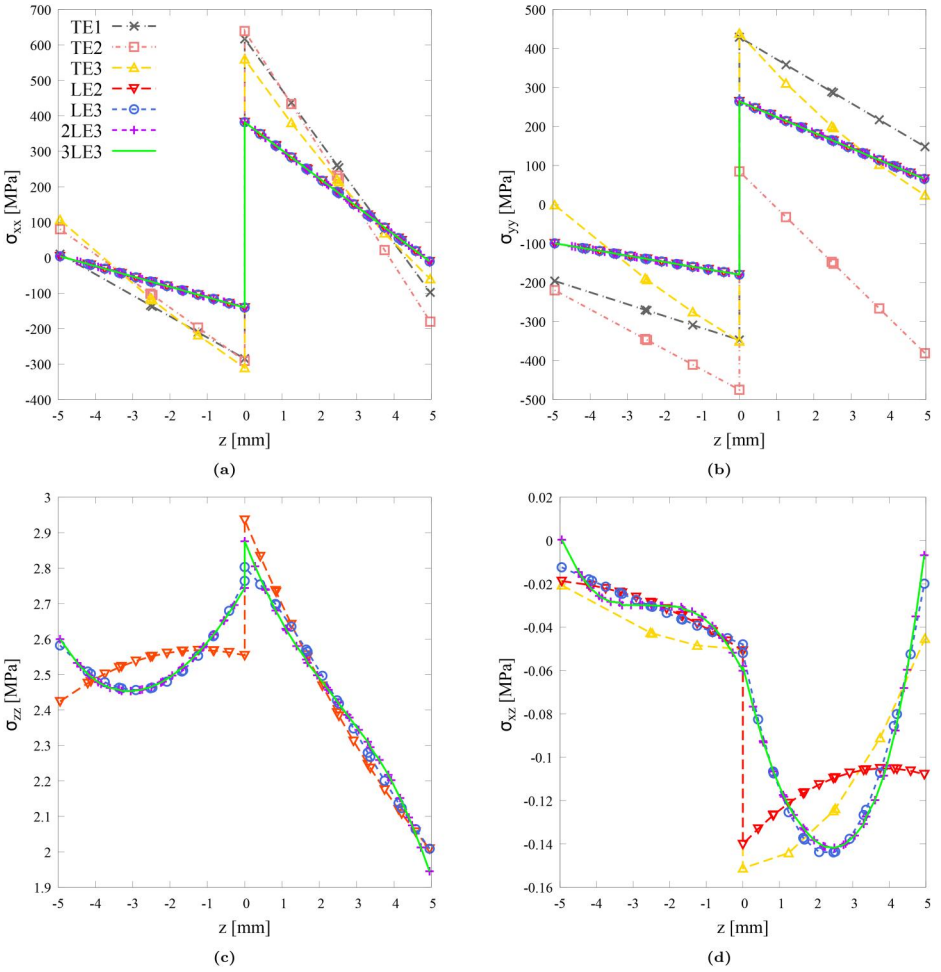


Figure 15. Stresses on the bimetallic plate, present method 20 × 10 Q9. Comparison of different model, $\Delta T = 200C^{\circ}$. results taken in point E.

Table 4. Stresses on the bimetallic plate evaluated in point E at $z = 2.5$ mm with $\Delta T = 200^{\circ}C$.

Theory	σ_{xx} [GPa]	σ_{yy} [GPa]	σ_{zz} [MPa]	σ_{xz} [MPa]	DOFs
TE1	0.2539	0.2863	0.2800×10^{3}	0.0752	12462
TE2	0.2277	0.2116	0.1038×10^{3}	−0.1241	18693
TE3	0.2135	0.1963	0.6525×10^{2}	−0.1237	24924
LE2	0.1823	0.1632	2.3834	−0.1093	31155
LE3	0.1823	0.1633	2.4183	−0.1435	43617
2LE3	0.1843	0.1643	2.4213	−0.1418	81003
3LE3	0.1843	0.1643	2.4213	−0.1418	118389

Classical plate theories may provide good displacement results, as seen in Figure 13. However, considering the stress results reported in Figure 15 and Table 4, it is clear that, also, for the in-plane stresses, it is necessary to use higher-order theories. Furthermore, to guarantee the continuity of the stress trend for the out-of-pane results, it is mandatory to use higher-order theories.

5. Conclusions

An investigation was made on nonlinear thermal stress and post-buckling induced by uniform temperature distribution. The governing equations are obtained through the principle of virtual displacement, where the thermo-elastic problem has been considered decoupled while the strains are expressed through the full Green-Lagrange strain tensor. The structural problem is described by efficient finite element formulation, which includes high-order theories and a description of the shear and volumetric strains implemented by the CUF. In such a manner, an accurate characterization of the post-buckling and large-displacement path is possible. Furthermore, the proposed methodology allows us to obtain a precise nonlinear description of the stress distribution caused by the thermal load. The governing equations obtained are independent of the study case, and it is demonstrated that the formulation is valid for each problem analyzed; in fact, a variety of results are obtained without any formal change in the problem formulation.

In the paper, different materials, shapes, and laminations are considered, and the displacement is compared to those of different publications. The displacement path is obtained by varying the applied overtemperature from low to high level. These displacements are compared with both published and Nastran 2D results. Both these comparisons constitute a verification for the presented model, which leads to an accurate description of the through-the-thickness stretching. Reliable results of displacements are already obtained through classical theories. The use of TE models with the ESL approach gives us an accurate description with a low computational cost, and TE1 and TE2 models are already thorough in obtaining displacement outcomes. When the problem is more complex, as in the analyzed bimetallic plate, the description of u_x and u_z demands at least the TE2 model.

In addition, the stress results are reported for some of these reference models. The present formulation allows us to easily obtain the 3D stress state in the plate. It is demonstrated that classical models cannot account for good stress results, particularly when out-of-plane stresses are considered. If the plate is nearly isotropic, the in-plane stresses can also be described through TE models. In contrast, Layer-Wise models are mandatory when anisotropy increases or when out-of-plane stresses have to be described. Layer-Wise models combined with refined theories are the only ones that can guarantee the interlaminar continuity of the out-of-plane stresses.

The investigation revealed that both the trend and the resulting stresses are influenced by nonlinear behavior. This is evidenced by the comparison between the results of the pre-buckling and post-buckling stresses. In contrast, it is known that in the linearized analysis, the trend remains unchanged, and by increasing the load, only the value of the result varies linearly.

Different convergence analyses are reported, and the optimum mesh for the analysis changes depending on the value of the applied load. Increasing the nonlinearity of the model, a denser mesh is necessary to ensure good stress results; instead, for the displacement results, a coarse mesh is enough for all the load levels.

Future works should account for temperature-dependent material properties with corresponding nonlinear effects. Furthermore, different thermal loadings should be considered.

Disclosure statement

The authors report there are no competing interests to declare.

ORCID

Alfonso Pagani http://orcid.org/0000-0001-9074-2558

Data availability statement

The data that support the findings of this study are available from the corresponding author A.P. upon reasonable request.

References

[1] J. Block, M. Straubel and M. Wiedemann, "Ultralight deployable booms for solar sails and other large gossamer structures in space," *Acta Astronaut.*, vol. 68, no. 7-8, pp. 984–992, Apr. 2011. DOI: 10.1016/j.actaastro.2010.09.005.

[2] J. Huang, "The development of inflatable array antennas," *IEEE Antennas Propag. Mag*, vol. 43, no. 4, pp. 44–50, 2001. DOI: 10.1109/74.951558.

[3] W. Guo, Y. Li, Y. Z. Li, S. Tian and S. Wang, "Thermal–structural analysis of large deployable space antenna under extreme heat loads," *J. Thermal Stresses*, vol. 39, no. 8, pp. 887–905, Jun. 2016. DOI: 10.1080/01495739.2016.1189776.

[4] S. Appel, *Simulation of Thermoelastic Behaviour of Spacecraft Structures. Springer Aerospace Technology*. Cham: Springer, 2022.

[5] M. Sathyamoorthy, *Nonlinear Analysis of Structures. Mechanical Engineering Series*. Boca Raton: CRC Press, 2017.

[6] P. F. Pai, *Highly Flexible Structures. AIAA Education Series*. Reston, VA: American Institute of Aeronautics and Astronautics, 2011.

[7] A. K. Noor and W. S. Burton, "Computational models for high-temperature multilayered composite plates and shells," *Appl. Mech. Rev.*, vol. 45, no. 10, pp. 419–446, Oct. 1992. DOI: 10.1115/1.3119742.

[8] L. Boni, A. A. Quarta and G. Mengali, "Thermal-structural analysis of a square solar sail," *Acta Astronautica*, vol. 154, pp. 268–277, Jan. 2019. DOI: 10.1016/j.actaastro.2018.03.037.

[9] C. Y. Chia, "Geometrically nonlinear behavior of composite plates: a review," *Appl. Mech. Rev.*, vol. 41, no. 12, pp. 439–451, Dec. 1988. DOI: 10.1115/1.3151873.

[10] E. F. Punch and S. N. Atluri, "Large displacement analysis of plates by a stress-based finite element approach," *Comput. Struct.*, vol. 24, no. 1, pp. 107–117, Jan. 1986. DOI: 10.1016/0045-7949(86)90339-1.

[11] I. Benedetti, V. Gulizzi and A. Milazzo, "X-ritz solution for nonlinear free vibrations of plates with embedded cracks," *Aerotec. Missili Spazio*, vol. 98, no. 1, pp. 75–83, Jan. 2019. DOI: 10.1007/s42496-019-00006-5.

[12] A. Pagani, M. Valente, R. Azzara and E. Carrera, "High-order effects on the vibration of membrane structures," *Mech. Adv. Mater. Struct.*, vol. 31, no. 30, pp. 13168–13181, Apr. 2024. DOI: 10.1080/15376494.2024.2334363.

[13] E. Carrera, "Transverse normal stress effects in multilayered plates," *J. Appl. Mech.*, vol. 66, no. 4, pp. 1004–1012, Dec. 1999. DOI: 10.1115/1.2791769.

[14] V. B. Tungikar and K. M. Rao, "Three dimensional exact solution of thermal stresses in rectangular composite laminate," *Compos. Struct.*, vol. 27, no. 4, pp. 419–430, Jan. 1994. DOI: 10.1016/0263-8223(94)90268-2.

[15] T. Kant and R. K. Khare, "Finite element thermal stress analysis of composite laminates using a higher-order theory," *J. Therm. Stresses*, vol. 17, no. 2, pp. 229–255, Apr. 1994. DOI: 10.1080/01495739408946257.

[16] J. W. Han, J. S. Kim and M. Cho, "New enhanced first-order shear deformation theory for thermo-mechanical analysis of laminated composite and sandwich plates," *Composites Part B Eng.*, vol. 116, pp. 422–450, May 2017. DOI: 10.1016/j.compositesb.2016.10.087.

[17] M. R. Prabhu and R. Dhanaraj, "Thermal buckling of laminated composite plates," *Comput. Struct.*, vol. 53, no. 5, pp. 1193–1204, Dec. 1994. DOI: 10.1016/0045-7949(94)90166-X.

[18] L. C. Shiau, S. Y. Kuo and C. Y. Chen, "Thermal buckling behavior of composite laminated plates," *Compos. Struct.*, vol. 92, no. 2, pp. 508–514, Jan. 2010. DOI: 10.1016/j.compstruct.2009.08.035.

[19] W. J. Chen, P. D. Lin and L. W. Chen, "Thermal buckling behavior of thick composite laminated plates under nonuniform temperature distribution," *Comput. Struct.*, vol. 41, no. 4, pp. 637–645, Jan. 1991. DOI: 10.1016/0045-7949(91)90176-M.

[20] K. R. Thangaratnam, Palaninathan and J. Ramachandran. Thermal buckling of composite laminated plates. *Comput. Struct.*, 32(5):1117–1124, Jan. 1989. DOI: 10.1016/0045-7949(89)90413-6.

[21] A. W. Leissa, "Conditions for laminated plates to remain flat under inplane loading," *Compos. Struct.*, vol. 6, no. 4, pp. 261–270, Jan. 1986. DOI: 10.1016/0263-8223(86)90022-X.

[22] M. S. Qatu and A. W. Leissa, "Buckling or transverse deflections of unsymmetrically laminated plates subjected to in-plane loads," *AIAA J.*, vol. 31, no. 1, pp. 189–194, Jan. 1993. DOI: 10.2514/3.11336.

[23] G. Singh, G. V. Rao and N. G. R. Lyengar, "Thermal postbuckling behavior of laminated composite plates," *AIAA J.*, vol. 32, no. 6, pp. 1336–1338, Jun. 1994. DOI: 10.2514/3.12143.

[24] M. K. Singha, L. S. Ramachandra and J. N. Bandyopadhyay, "Thermal postbuckling analysis of laminated composite plates," *Compos. Struct.*, vol. 54, no. 4, pp. 453–458, Dec. 2001. DOI: 10.1016/S0263-8223(01)00117-9.

[25] V. M. Sreehari and D. K. Maiti, "Buckling and post buckling analysis of laminated composite plates in hygrothermal environment using an inverse hyperbolic shear deformation theory," *Compos. Struct.*, vol. 129, pp. 250–255, Oct. 2015. DOI: 10.1016/j.compstruct.2015.04.010.

[26] L. W. Chen and L. Y. Chen, "Thermal postbuckling behaviors of laminated composite plates with temperature-dependent properties," *Compos. Struct.*, vol. 19, no. 3, pp. 267–283, Jan. 1991. DOI: 10.1016/0263-8223(91)90031-S.

[27] N. N. Huang and T. R. Tauchert, "Postbuckling response of antisymmetric angle-ply laminates to uniform temperature loading," *Acta Mechanica*, vol. 72, no. 1-2, pp. 173–183, May 1988. DOI: 10.1007/BF01176551.

[28] C. A. Meyers and M. W. Hyer, "Thermal buckling and postbuckling of symmetrically laminated composite plates," *J. Thermal Stresses*, vol. 14, no. 4, pp. 519–540, Oct. 1991. DOI: 10.1080/01495739108927083.

[29] B. Wu, A. Pagani, M. Filippi, W. Q. Chen and E. Carrera, "Large-deflection and post-buckling analyses of isotropic rectangular plates by Carrera Unified Formulation," *Int. J. Non-Linear Mech.*, vol. 116, pp. 18–31, Nov. 2019. DOI: 10.1016/j.ijnonlinmec.2019.05.004.

[30] S. K. Panda and B. N. Singh, "Thermal postbuckling behavior of laminated composite spherical shell panel using NFEM$^{\#}$," *Mech. Based Des. Struct. Mach.*, vol. 41, no. 4, pp. 468–488, Oct. 2013. DOI: 10.1080/15397734.2013.797330.

[31] E. Carrera, E. Zappino, M. Cinefra and M. Petrolo, *Finite Element Analysis of Structures through Unified Formulation*. Chichester, West Sussex: Wiley, 2014,

[32] E. Carrera, F. A. Fazzolari and M. Cinefra, *Thermal Stress Analysis of Composite Beams, Plates and Shells*. Amsterdam: Joe Hayton, 2017.

[33] R. Vescovini and L. Dozio, "A variable-kinematic model for variable stiffness plates: vibration and buckling analysis," *Compos. Struct.*, vol. 142, pp. 15–26, May 2016. DOI: 10.1016/j.compstruct.2016.01.068.

[34] F. Bracaglia, R. Masia, A. Pagani, E. Zappino and E. Carrera, "Thermal buckling of variable stiffness composite laminates using high order plate finite elements," *Compos. Struct.*, vol. 345, pp. 118393, Oct. 2024. DOI: 10.1016/j.compstruct.2024.118393.

[35] S. S. Rao, *The Finite Element Method in Engineering*. Amsterdam: Elsevier, 2011.

[36] K. Washizu, *Variational Methods in Elasticity and Plasticity*. Oxford: Pergamon, 1968.

[37] A. Pagani and E. Carrera, "Unified formulation of geometrically nonlinear refined beam theories," *Mech. Adv. Mater. Struct.*, vol. 25, no. 1, pp. 15–31, Sep. 2018. DOI: 10.1080/15376494.2016.1232458.

[38] J. N. Reddy, *An Introduction to Nonlinear Finite Element Analysis*, 2nd ed., first published in paperback edition. Oxford: Oxford University, 2020.

[39] M. A. Crisfield, "An arc-length method including line searches and accelerations," *Numer. Methods Eng.*, vol. 19, no. 9, pp. 1269–1289, Sep. 1983. DOI: 10.1002/nme.1620190902.

[40] E. Carrera, "A study on arc-length-type methods and their operation failures illustrated by a simple model," *Comput. Struct.*, vol. 50, no. 2, pp. 217–229, Jan. 1994. DOI: 10.1016/0045-7949(94)90297-6.

[41] B. J. Matkowsky, L. J. Putnick and E. L. Reiss, "Secondary states of rectangular plates," *SIAM J. Appl. Math.*, vol. 38, no. 1, pp. 38–51, Feb. 1980. DOI: 10.1137/0138003.

[42] G. Li, *et al.*, "Evaluation of shear and membrane locking in refined hierarchical shell finite elements for laminated structures," *Adv. Model. Simul. Eng. Sci.*, vol. 6, no. 1, pp. 8, May 2019. DOI: 10.1186/s40323-019-0131-1.

[43] P. Chiaia, A. Pagani and E. Carrera, "Large strain and 3D stress analysis of laminated fiber-reinforced soft material structures with high order beam finite elements," *Comput. Struct.*, vol. 313, pp. 107735, Jun. 2025. DOI: 10.1016/j.compstruc.2025.107735.

Appendix A.
Explicit formulation of B^*_{nl}

Hereafter, it is reported the matrix B^*_{nl} employed in the building of the tangent stiffness matrix. The full derivation of the matrix is not here reported but can be found in the literature [37].

$$\boldsymbol{B}^*_{nl} = \begin{bmatrix} F_\tau N_{i,x} F_s N_{j,x} & F_\tau N_{i,x} F_s N_{j,x} & F_\tau N_{i,x} F_s N_{j,x} \\ F_\tau N_{i,y} F_s N_{j,y} & F_\tau N_{i,y} F_s N_{j,y} & F_\tau N_{i,y} F_s N_{j,y} \\ F_{\tau,z} N_i F_{s,z} N_j & F_{\tau,z} N_i F_{s,z} N_j & F_{\tau,z} N_i F_{s,z} N_j \\ F_\tau N_{i,x} F_{s,z} N_j + F_{\tau,z} N_i F_s N_{j,x} & F_\tau N_{i,x} F_{s,z} N_j + F_{\tau,z} N_i F_s N_{j,x} & F_\tau N_{i,x} F_{s,z} N_j + F_{\tau,z} N_i F_s N_{j,x} \\ F_\tau N_{i,y} F_{s,z} N_j + F_{\tau,z} N_i F_s N_{j,y} & F_\tau N_{i,y} F_{s,z} N_j + F_{\tau,z} N_i F_s N_{j,y} & F_\tau N_{i,y} F_{s,z} N_j + F_{\tau,z} N_i F_s N_{j,y} \\ F_\tau N_{i,x} F_s N_{j,y} + F_\tau N_{i,y} F_s N_{j,x} & F_\tau N_{i,x} F_s N_{j,y} + F_\tau N_{i,y} F_s N_{j,x} & F_\tau N_{i,x} F_s N_{j,y} + F_\tau N_{i,y} F_s N_{j,x} \end{bmatrix} \tag{53}$$

In the present matrix F_τ and F_s denote the expansion functions, N_i and N_j are referred to the shape functions and the subscript ',' stands for the derivative.